Pharmacological Research 195 (2023) 106858

Contents lists available at ScienceDirect

Pharmacological Research

journal homepage: www.elsevier.com/locate/yphrs

Targeting GLI1 and GLI2 with small molecule inhibitors to suppress GLI-dependent transcription and tumor growth

Luisa Maresca [a], Enrica Crivaro [a,b], Francesca Migliorini [b], Giulia Anichini [a], Alessandro Giammona [a], Sara Pepe [a], Federica Poggialini [b], Chiara Vagaggini [b], Giuseppe Giannini [c], Serena Sestini [d], Lorenzo Borgognoni [d], Andrea Lapucci [e], Elena Dreassi [b], Maurizio Taddei [b], Fabrizio Manetti [b,*], Elena Petricci [b,*], Barbara Stecca [a,**]

[a] Core Research Laboratory - Institute for Cancer Research and Prevention (ISPRO), Florence, Italy
[b] Dept. of Biotechnology, Chemistry and Pharmacy, University of Siena, Siena, Italy
[c] R&D, Alfasigma SpA, Roma, Italy
[d] Plastic and Reconstructive Surgery Unit Regional Melanoma Referral Center and Melanoma & Skin Cancer Unit, Santa Maria Annunziata Hospital, Florence, Italy
[e] Department of Health Sciences, University of Florence, Florence, Italy

ARTICLE INFO

Keywords:
GLI transcription factors
Small molecule inhibitors
Cancer
Melanoma

ABSTRACT

Aberrant activation of Hedgehog (HH) signaling in cancer is the result of genetic alterations of upstream pathway components (canonical) or other oncogenic mechanisms (noncanonical), that ultimately concur to activate the zinc-finger transcription factors GLI1 and GLI2. Therefore, inhibition of GLI activity is a good therapeutic option to suppress both canonical and noncanonical activation of the HH pathway. However, only a few GLI inhibitors are available, and none of them have the profile required for clinical development due to poor metabolic stability and aqueous solubility, and high hydrophobicity. Two promising quinoline inhibitors of GLI were selected by virtual screening and subjected to hit-to-lead optimization, thus leading to the identification of the 4-methoxy-8-hydroxyquinoline derivative JC19. This molecule impaired GLI1 and GLI2 activities in several cellular models interfering with the binding of GLI1 and GLI2 to DNA. JC19 suppressed cancer cell proliferation by enhancing apoptosis, inducing a strong anti-tumor response in several cancer cell lines *in vitro*. Specificity towards GLI1 and GLI2 was demonstrated by lower activity of JC19 in GLI1- or GLI2-depleted cancer cells. JC19 showed excellent metabolic stability and high passive permeability. Notably, JC19 inhibited GLI1-dependent melanoma xenograft growth *in vivo*, with no evidence of toxic effects in mice. These results highlight the potential of JC19 as a novel anti-cancer agent targeting GLI1 and GLI2.

1. Introduction

Aberrant activation of the Hedgehog (HH) pathway has been associated to tumorigenesis [1]. Canonical activation of the HH pathway is triggered by the binding of HH ligands (Sonic, Indian, and Desert) to the Patched (PTCH) receptor, which relieves the repression on the G protein-coupled receptor Smoothened (SMO). SMO transduces the signals to the downstream zinc-finger (ZF) transcription factors GLI1 and GLI2, which regulate the expression of HH target genes [2]. GLI are C2H2-type transcription factors that contain five ZF regions, in which ZF2-ZF5 wrap around the full helical turn of the DNA, whereas ZF1 does not directly interact with the DNA. The most important domains for recognition of the conserved DNA consensus sequence 5'-GACCACCCA-3' are ZF4 and ZF5, whereas ZF1-ZF3 bind the phosphate backbone and contribute to the control of binding stability [3,4].

HH-driven cancers (medulloblastoma and basal cell carcinoma) harbor upstream activation of the HH pathway, either through loss-of-function of PTCH1 or gain-of-function of SMO [5]. Moreover, several types of cancer present SMO-independent noncanonical activation of the downstream GLI transcription factors through multiple oncogenic inputs, such as mTOR/S6K1, aPKC ι/λ, BET proteins, MEK/ERK, DYRK1A/B, CK1 and CK2 kinases, and loss of SNF5 or p53 [6–17]. Other GLI-activating mechanisms involve decreased ubiquitination-mediated degradation and deacetylation [18–22]. All of these mechanisms lead

* Corresponding authors.
** Correspondence to: Core Research Laboratory – Institute for Cancer Research and Prevention (ISPRO), Viale Pieraccini 6, 50139 Florence, Italy.
E-mail addresses: fabrizio.manetti@unisi.it (F. Manetti), elena.petricci@unisi.it (E. Petricci), b.stecca@ispro.toscana.it (B. Stecca).

https://doi.org/10.1016/j.phrs.2023.106858
Received 24 February 2023; Received in revised form 17 July 2023; Accepted 17 July 2023
Available online 19 July 2023

to high GLI protein levels or active forms that interact with the DNA of target genes, thus enhancing transcription. Therefore, with their roles as downstream effectors of multiple oncogenic signaling pathways, the GLI represent a unique and promising drug targets for a variety of human tumors beyond the HH-dependent cancers. SMO inhibitors have been approved by the FDA [23] or are under investigation by our group and others [24–26] for the treatment of different cancers. However, SMO inhibitors cause drug resistance that might be overcome by developing negative modulators of the downstream effectors GLI. Unfortunately, the identification and development of small molecules directly targeting the GLI proteins has progressed very slowly over the years, and only a few GLI inhibitors have been identified so far [27,28]. To date, GANT61, arsenic trioxide (ATO) and Glabrescione B (GlaB) are the only direct GLI antagonists identified. ATO has been described to prevent ciliary accumulation of GLI2 enhancing its degradation, and to bind to GLI1 protein and inhibit its transcriptional activity [29,30]. Although ATO was approved by FDA for treatment of acute promyelocytic leukemia, it is not specific for the GLI transcription factors. GANT61 and GlaB have been reported to directly bind GLI1 and inhibit the canonical and non-canonical HH pathway [31,32]. However, neither of them has the profile suitable for clinical development [33–36]. The activity of GANT61 is moderate, with micromolar concentrations required for *in vitro* inhibition. In addition, GANT61 is rapidly hydrolyzed into a diamine derivative [37], which is predicted to maintain its ability to bind GLI [38,39]. More recently, the natural isoflavone GlaB was reported as a GLI1 inhibitor that interferes with the GLI1/DNA binding [32]. Nevertheless, GlaB is characterized by poor aqueous solubility [40]. To fill this gap, we have previously applied a virtual screening approach [41,42] that led to the identification of a series of quinoline derivatives as promising small molecule inhibitors of GLI1 that can inhibit GLI-mediated transcription and tumor growth. Such compounds have a suitable structure for further optimization and have been used to design and synthesize next-generation compounds with the aim of enhancing their activity and improving their metabolic profile.

Here, we describe the results of an in-depth biological evaluation of three quinolines that led to the identification of a small molecule with drug-like properties (JC19) for the treatment of tumors with hyperactivation of GLI1 and GLI2 TFs. JC19 directly targets GLI1 and GLI2, preventing the binding of the two TFs to DNA. Furthermore, JC19 shows antiproliferative activity against several tumor cell lines, has good pharmacokinetics parameters, and inhibits GLI-dependent melanoma xenograft growth *in vivo*, thus representing a promising candidate for further evaluation as an anti-tumor agent.

2. Materials and methods

2.1. Molecular docking simulations

A virtual screening approach [41,42] based on the use of the software Phase (pharmacophore modeling) and Glide (molecular docking) within the Schrödinger suite (Schrödinger Release 2019–2, Schrödinger, LLC, New York, NY, 2019) previously led us to prioritize three different classes of compounds among the chemical entries of the commercially available databases of compounds Asinex (Asinex Corporation, www.asinex.com) and AKos (AKos Consulting & Solutions GmbH, http://www.akosgmbh.de). Among these, quinoline derivatives were selected as putative GLI1 inhibitors [42].

The structures of the quinoline derivatives reported herein were sketched with LigPrep by using the OPLS3e force field. Epik software was also applied to generate ionized and tautomeric forms at pH 7 ± 1. Conformational sampling of each compound was performed with a systematic pseudo Monte Carlo algorithm by retaining conformers within 25 kcal/mol from the minimum. The Protein Preparation Wizard was applied for the optimization of the three-dimensional structure of the complex between the five-finger GLI1 and a DNA fragment (protein data bank entry 2gli, 2.6 Å resolution). Next, two putative binding sites at ZF4 and between ZF1 and ZF3 were identified using SiteMap (binding site identification) and used for docking simulations (Glide software). Ligands were docked as flexible structures using the extra-precision mode, by collecting ten poses per ligand that were minimized by the application of default parameters.

2.2. Synthesis

The methods and reaction schemes for the large-scale synthesis of SST0776, SST0794, and JC19 are reported in Supporting Materials and Methods.

2.3. Cell lines

Human melanoma cells A375 (ATCC cat# CRL-1619), MeWo (ATCC cat# HTB-65) and SK-Mel-5 (ATCC cat# HTB-70), breast cancer cells MCF-7 (ATCC cat# HTB-22), glioblastoma cells U87-MG (ATCC cat# HTB-14), medulloblastoma cells Daoy (ATCC cat# HTB-186), HEK-293 T cells (ATCC cat# CRL-3216), and murine NIH3T3 cells (ATCC cat# CRL-1658) were obtained from ATCC (Manassas, VA, USA). Cholangiocarcinoma cells CCLP1 and HuCCT1 were kindly provided by Dr. Chiara Raggi (University of Florence, Italy). Cells were maintained in Dulbecco's modified Eagle's medium (DMEM) (Euroclone, Milan, Italy), Eagle's Mininum Essential Medium (EMEM) (Euroclone) or RPMI-1640 medium supplemented with 10% fetal bovine serum (FBS), 1% Penicillin-Streptomycin, and 1% Glutamine (Lonza, Basel, Switzerland). Me53 short-term melanoma culture was established as previously described [43] from a metastatic nodular cutaneous melanoma (female, age 88) obtained from Plastic and Reconstructive Surgery Unit of the S. M. Annunziata Hospital (Florence, Italy) after written consent and approved protocol by the local Independent Ethical Committee (Comitato Etico Regionale per la Sperimentazione Clinica della Regione Toscana, Area Vasta Centro; Protocol 16922_bio). Patient-derived SSM2c [43] and Me53 cells were grown in DMEM/F12 (Euroclone) supplemented with 10% FBS, 2% Penicillin-Streptomycin, 1% Glutamine (Lonza), and EGF (5 ng/mL) (Life Technologies, Paisley, UK). *Ptch1-/-* and *SuFu-/-* MEFs were kindly provided by Prof. Lucia Di Marcotullio (University La Sapienza, Rome, Italy), and were cultured in DMEM with 10% FBS, 1% Penicillin-Streptomycin and 1% Glutamine. MCF10A cells (ATCC cat# CRL-10317) were a kindly provided by Dr. Silvestro Conticello (CRL-ISPRO, Florence, Italy) and were maintained in DMEM/F12 (Euroclone) supplemented with 5% horse serum, 1% Penicillin-Streptomycin, 1% Glutamine (Lonza), 100 ng/mL cholera toxin, 10 μg/mL insulin, 20 ng/mL hEGF and 500 ng/mL hydrocortisone. Normal human epidermal melanocytes (NHEM, cat# C-12400) were obtained from PromoCell (Heidelberg, Germany) and cultured in Melanocyte Growth Medium (PromoCell). Cells were periodically screened for *Mycoplasma* contamination using PCR.

2.4. Drugs

SST0776 and SST0794 were purchased from Asinex, and AKos vendors, respectively.

Glabrescione B (GlaB) was kindly provided by Prof. Lucia di Marcotullio and Prof. Bruno Botta (University La Sapienza, Rome, Italy). Puromycin, blasticydine, doxycycline, GANT61, SAG and MG132 were purchased from Sigma-Aldrich (St. Louis, MO). Mithramycin was obtained from Merck Millipore (Burlinghton, MA).

2.5. Cell viability assay

Cells were plated in 24-well or 96-well plates and treated with increasing concentrations of the three GLI inhibitors, GlaB, or DMSO as a control, in complete medium supplemented with 1% FBS. After 72 h, cells were fixed with 4% PFA and stained with crystal violet. The cells were then de-stained with 10% acetic acid, and the absorbance was read

at 590 nm on Victor X5 (Perkin Elmer). IC_{50} values were calculated using GraphPad Prism v7 software (GraphPad Prism).

2.6. Luciferase reporter assays

The GLI-responsive luciferase reporter plasmid (8 ×3' Gli-BS) [41] was used in combination with *Renilla* luciferase pRL-TK reporter vector (Promega, Madison, WI) to normalize luciferase activities, and the pGL3Basic vector (Promega) was used to normalize DNA amounts. Luminescence was measured using the Dual-Glo Luciferase Assay System (Promega) and GloMax 20/20 Luminometer (Promega).

2.7. Plasmid construction, mutagenesis, retroviral and lentiviral vectors

Lentiviral particles for gene silencing were produced using HEK-293 T cells as previously described [43]. The shRNA vectors used were: pLKO.1-puro (LV-c), pLKO.1-puro-shGLI1 (LV-shGLI1) [43], and pLKO.1-puro-shGLI2 (LV-shGLI2) [44]. Retroviruses for gene overexpression were produced in HEK-293 T cells co-transfected with pBABE-puro (LV-c), pBABE-puro-GLI1 (LV-GLI1), or pBABE-puro-GLI2 (LV-GLI2) with pUMVC packaging vector and pMD2.G envelope vector. pBABE-puro-GLI1 and pBABE-puro-GLI2 were obtained by amplifying the coding sequences of Myc-tagged human GLI1 and GLI2 (pCS2+MT-GLI1 and pCS2+MT-GLI2, respectively) [44]. PCR products were then cloned into pBABE-puro using *Sna*BI and *Eco*RI restriction sites. The primers used for cloning were (5' to 3'): GLI1 clonF: ttttttacgtaATGTTCAACTCGATGACCCCAC, GLI1 clonR: tttttgaattcTTAGGCACTAGAGTTGAGGAA, GLI2 clonF: tttttacgtaATGGAGACGTCTGCCTCAGC, GLI2 clonR: ttttgaattcCTAGGTCATCATGTTCAGGAAC. Mutations of GLI1 ZF4 and ZF5 were introduced using QuikChange II (Agilent Technologies, Santa Clara, CA, USA) with the following primers (5' to 3'): H351A F: GTGACCGAGCCAAGGCCCAGAATCGGACCC, H351A R: GGGTCCGATTCTGGGCCTTGGCTCGGTCAC, R354A F: CCGAGCCAAGCACCAGAATGCGACCCATTCCAAT, R354A R: ATTGGAATGGGTCGCATTCTGGTGCTTGGCTCGG,

T355A F: CCAAGCACCAGAATCGGGCCCATTCCAATGAGAAG, T355A R: CTTCTCATTGGAATGGGCCCGATTCTGGTGCTTGG, H356A F: GCACCAGAATCGGACCGCTTCCAATGAGAAGCCG, H356A R: CGGCTTCTCATTGGAAGCGGTCCGATTCTGGTGC, T374A F: CTGCACCAAACGCTATGCAGATCCTAGCTCGC, T374A R: GCGAGCTAGGATCTGCATAGCGTTTGGTGCAG.

pCW-Cas9 and pLX-sgRNA were kindly provided by Dr. Laura Poliseno (CNR, Pisa, Italy). pLX-sgRNA-GLI1 was produced by PCR from pLX-sgRNA (scrambled sgRNA) according to the protocol available at https://www.addgene.org/50662/ [45]. The primers used were (5' to 3'): CommonF1: AAACTCGAGTGTACAAAAAAGCAGGCTTTAAAG, CommonR2: AAAGCTAGCTAATGCCAACTTTGTACAAGAAAGCTG, sgRNAGLI1F2: GCGAGTTGATGAAAGCTACGGTTTTAGAGCTAGAAATAGCAA, sgRNAGLI1F1: CGTAGCTTTCATCAACTCGCGGTGTTTCGTCCTTTCC. The PCR product was cloned into pLX-sgRNA using *Xho*I and *Nhe*I restriction sites. Lentiviral particles for CRISPR-Cas9 were produced by co-transfecting pCW-Cas9 or pLX-sgRNA-GLI1 with the dR8.74 packaging vector and pMD2.G envelope vector.

2.8. GLI1 CRISPR-Cas9

To generate a GLI1 knockout, pCW-Cas9 and pLX-sgRNA-GLI1 were stably expressed into U87-MG cells. Transduced cells were treated with 1 μg/mL doxycycline (Sigma) to induce Cas9 expression, and 48 h later, the cells were seeded in 96 well plate to isolate individual clones. Knockout was verified by Western blot. It was not possible to obtain viable GLI1 ko clones. The bulk population obtained after 48 h of doxycycline treatment was used in the experiments.

2.9. Quantitative real-time PCR

Total RNA was isolated using the TriPure Isolation Reagent (Roche Diagnostics, Basel, Switzerland), subjected to DNase I treatment (Roche Diagnostics). Reverse transcription was performed using High-Capacity cDNA Reverse Transcription Kit (Applied Biosystems, Carlsbad, CA, USA). qPCR amplifications were carried out at 60 °C using FastStart SYBR Green Master (Roche Diagnostics) in a Rotorgene-Q. Primer sequences used for qPCR are listed in Supporting Table S1.

2.10. Chromatin immunoprecipitation

Chromatin Immunoprecipitation (ChIP) experiments were performed using EZ-Magna ChIP A/G Kit (Millipore, cat.17–10086) according to the manufacturer's instructions, as previously reported [46]. Chromatin fragments were then immunoprecipitated at 4 °C overnight using mouse anti-GLI1 (Cell Signaling Technology cat#2643) or goat anti-GLI2 (R&D Systems cat#AF3635) antibodies. Normal mouse IgG (Millipore) was used as a negative control. qPCR was performed as described above. The primers used for ChIP-qPCR were as follows (5' to 3'): PTCH1promF: CTGTCAGATGGCTTGGGTTT; PTCH1promR: GCCTACCTGGGTGGTCTCTC.

2.11. Electrophoretic mobility-shift assay (EMSA)

EMSA was performed using EMSA Kit with SYBR™ Green & SYPRO™ Ruby stains (Thermo Fisher Scientific) according to manufacturer's instructions. HEK-293 T cells overexpressing GLI1 were lysed in cytoplasmic Buffer A supplemented with protease and phosphatase inhibitors and subsequently in RIPA buffer. The complementary oligonucleotides for GLIBS (GLIBS F: TTGCCTACCTGGGTGGTCTCTCTACTT; GLIBS R: AAGTAGAGAGACCACCCAGGTAGGCAA) were annealed for 10 min at 95 °C and cooled down to rt. The probe obtained was then incubated with 20 μg of nuclear extract in binding buffer for 20 min at rt. Samples were resolved on a Native 6% PAGE. ChemiDoc XRS (Bio-Rad, Hercules, CA, USA) was used for SYBR Green detection.

2.12. DNA pull-down

The biotin-labeled probe GLIBS probe TTGCCTACCTGGGTGGTCTCTCTACTT was used in DNA pull-down assays. Briefly, the Dynabeads MyOne Streptavidin T1 (Thermo Fisher Scientific) magnetic beads were washed three times in the B&W buffer according to manufacturer's instructions. Then 150 μg of whole cell lysate from HEK-293 T cells transiently transfected with Myc-tagged human GLI1 (pCS2+MT-GLI1) or pCS2+MT as a control [44] were preincubated with 200 pmol of the annealed 3' biotin-labeled GLIBS probe in presence of JC19 at 50 μM or 100 μM in 100 μL of RIPA buffer for 1 h at rt. Subsequently 50 μL of Dynabeads MyOne Streptavidin T1 and 400 μL of RIPA buffer were added to the samples for 1 h in rotation at rt. Following the incubation, the beads-probe-protein complexes were washed three times in RIPA buffer. After the complete removal of RIPA buffer, 25 μL of a 2xSDS-PAGE sample buffer were added to the beads and heated at 95 °C for 10 min for the elution of the protein binding complex. Samples were finally resolved on a 8% SDS-PAGE and analyzed by Western blot.

2.13. Western blot analysis

For Western blot analysis, cells were lysed in cold RIPA buffer (1% NP-40, 150 mM NaCl, 5 mM EDTA, 0.25% NaDOC, 50 mM Tris-HCl pH 7.5, 0.1% SDS) supplemented with protease and phosphatase inhibitors and processed as previously described [44]. The primary antibodies used in this study are listed in Supporting Table S2. ChemiDoc XRS (Bio-Rad) was used for chemiluminescence detection.

2.14. Flow cytometric analysis

Apoptosis was analyzed using the Annexin V-PE/7-AAD apoptosis kit (BD Biosciences, San Jose, CA, USA), according to the manufacturer's instructions. The percentages of both early (Annexin V+/7-AAD−) and late (Annexin V+/7-AAD+) apoptotic cells were detected and measured using CytoFLEX S (BD Beckman Coulter).

2.15. Caspase activity assay

Analysis of caspase 3 and 7 activities was performed using the Caspase-Glo 3/7 Assay System (Promega) according to the manufacturer's instructions.

2.16. In vitro ADME assays

All solvents and reagents were from Sigma-Aldrich (Milan, Italy). Dodecane was purchased from Fluka (Milan, Italy). Pooled male human liver microsomes were from BD Gentest-Biosciences (San Jose, CA). LC analyses for ADME studies were performed by UV/LC-MS with Agilent 1260 Infinity HPLC-DAD interfaced with an Agilent MSD 6130 (Agilent Technologies, Palo Alto, CA). Chromatographic separation was obtained using a Phenomenex Kinetex C18–100 Å column (150 ×4.6 mm) with 5 μm particle size and gradient elution with a binary solution; (eluent A: H_2O, eluent B: acetonitrile, both eluents were acidified with formic acid 0.1% v/v) at rt. The analysis started with 100% of A (from t = 0 to t = 3 min), then B was increased to 95% (from t = 3 to t = 10 min), then kept at 95% (from t = 10 to t = 12 min), and finally return to 100% of eluent A in 3.0 min and kept with this percentage for other 2 min. The flow rate was 0.6 mL/min, injection volumes were 10 μL, and UV detection was at 254 nm.

For aqueous solubility, solid compounds (1 mg) were added to 1 mL of distilled water or buffer solution (HEPES 25 mM, NaCl 140 mM, pH 7.4). The solution obtained was stirred at rt using a shaker water bath overnight. The resulting suspension was filtered through a 0.45 μm nylon filter, the quantification of the solubilized compound was carried out in triplicate using the HPLC-UV/MS method reported above, by comparing it with the appropriate calibration curve obtained from samples of the compound dissolved in an appropriate solvent at known concentrations.

For parallel artificial membrane permeability assay (PAMPA), from a stock solution of the compounds (1 mM in DMSO) a "donor solution" was prepared diluting 1:1 v/v with phosphate buffer (25 mM, pH 7.4) to a final concentration of 500 μM. Filters were coated with 10 μL of 1% w/v dodecane solution of phosphatidylcholine. The donor wells were filled with 150 μL of "donor solution" and the lower ones were filled with 300 μL of "acceptor solution" consisting of 50% v/v DMSO and phosphate buffer. The sandwich plate was assembled and incubated for 5 h at rt under gentle shaking. After the incubation time, the plates were separated, samples were collected from donor and acceptor wells and the amount of compound was quantified by HPLC-UV/MS. The determination of the compound was performed in three independent experiments. Permeability (P_{app}) and membrane retention percentage (MR%) were calculated using equations previously reported [47,48].

For stability test in human plasma, compounds (2.0 mM in DMSO) were incubated with pooled human plasma (55.7 μg protein/mL) and HEPES buffer (25 mM, 140 mM NaCl, pH 7.4) up to a final volume of 2.0 mL. The solution was mixed in a test tube that was incubated at 37 °C and at set time points (0.0, 0.08, 0.25, 0.50, 1, 2, 4, 8, 24 h) samples of 100 μL were taken, mixed with 400 μL of cold acetonitrile, centrifuged at 5000 rpm for 15 min, and the supernatant was removed and analyzed using the HPLC-UV/MS method previously described. The determination of the compound was performed in three independent experiments.

For metabolic stability in HLMs (Human Liver Microsomes), DMSO solution of the compounds was incubated for 1 h at 37 °C in buffer solution (PBS, 25 mM, pH 7.4) in presence of HLMs (0.2 mg/mL, 5 μL) and NADPH-generating system up to the final volume of 500 μL and final compounds concentration of 50 μM. The reaction was stopped by adding cold acetonitrile (1.0 mL) and cooling in ice. The reaction mixture was centrifuged, and the supernatant was taken, dried under nitrogen flow, and resuspended in 100 μL of methanol and the parent compound and its metabolites were determined by HPLC-UV/MS. The percentage of the unmetabolized compound was calculated by comparing reference solutions, and the determination was performed in three independent experiments.

For human serum albumin (HSA) binding assay, JC19 at C_{max} (1570 μg/mL) obtained after its *in vivo* administration at 25 mg/kg was incubated with human serum albumin [49] (0.615 mmol/L human serum in PBS 1 mM pH 7.4) to final volume of 0.5 mL for 30 min at 37 °C, and centrifuged for 10 min at 5000 rpm using Amicon filter units (membrane pore size 30,000 molecular weight cut-off). The filtered volume was collected and then analyzed using LC-UV-MS method described above. The percentage of unbound compound was calculated by comparison with reference solutions.

2.17. In vivo PK and BD Studies

Animal care and experimental procedures in this study complied with the WMA Statement on animal use in biomedical research and were carried out following ARRIVE guidelines [50,51] and EU recommendations (Directive 2010/63/EU) for experimental design and analysis in pharmacological care. In vivo PK and BD procedures performed in this study were approved by Institutional Animal Use and Care Committee at the University of Siena and authorized by the Italian Ministry of Health (Authorization n. 412/2016-PR). 4-week-old naive male BALB/C mice (Charles River, Milan, Italy) were maintained under pathogen-free conditions and given food and water *ad libitum*. For *in vivo* administration, JC19 was dissolved in a mixture of 10% DMSO in PBS and administered intraperitoneal (i.p.) as a single dose of 15 or 25 mg/kg in 100 μL volume. At several time points (0.08, 0.25, 0.5, 1, 2, 4, 8, 24 h) after JC19 administration, mice were treated i.p. with heparin (5000 U/kg) and sacrificed under CO_2. Six animals were used for each time point. Blood and liver were collected for the quantitative analysis. Approximately 500 μL of blood was collected from each animal and transferred to a tube containing 10 μL of heparin and mixed briefly to avoid the coagulation process.

For samples preparation, blood was centrifuged at 5000 rpm for 10 min and 200 μL of the plasma fractions were measured and collected. Acetonitrile (1500 μL) with SST0776 chosen as internal standard at the final concentration of 2.5 μg/mL, was added to the fractions to denature proteins. Liver (200 mg) was homogenized in presence of acetonitrile internal standard solution to extract the compound, with T10 basic ULTRA-TURRAX® homogenizer (Bioclass, Pistoia, Italy). After centrifugation at 5000 rpm for 10 min, supernatants were recovered and analysed by HPLC-UV/MS. The pharmacokinetic parameters, including area under the concentration-time curve (AUC), maximum plasma concentration (C_{max}), half-time ($t_{1/2}$), apparent volume of distribution (V), plasma clearance (CL), and mean residence time (MRT), were calculated by non-compartmental analysis using PKSolver software.

2.18. Human melanoma xenografts

Exponentially growing A375 cells were resuspended in a mixture of 50% Matrigel (Merck, cat#CLS356234) and 50% DMEM and injected subcutaneously into both lateral flanks of adult (7–8 weeks) female athymic nude mice strain Crl:NU(NCr)-*Foxn1*^{nu} (Charles River Laboratories, Italy) (1 ×10^5 cells/injection). Once the tumors were palpable (approximately 20 mm^3), mice were randomized into three groups (n = 10 per group) and treated i.p. with JC19 (15 mg/kg, BID), JC19 (25 mg/kg, BID), or vehicle (10% DMSO in PBS, BID) for 12 days. During the experiment, investigators were not blinded. Mice were checked daily for signs of illness and distress. The subcutaneous tumor size and mouse

weight were measured three times per week. The mice were maintained under pathogen-free conditions and with free access to standard rodent chow and water. For pharmacodynamic studies on tumor samples, tumor-bearing mice were treated with JC19 or vehicle for three days. Animals were euthanized 3 h after the last treatment, and the tumors were dissected and snap-frozen. Animal procedures were performed according to the study protocol approved by the Institutional Animal Use and Care Committee at the University of Florence and the Italian Ministry of Health (authorization n. 155/2020-PR).

2.19. Statistical analysis

Data represent mean ± SD or mean ± SEM values calculated on at least three independent experiments. No statistical methods were used for the sample size selection. P-values were calculated using Student's t-test (two groups) or one-way analysis of variance (ANOVA) (more than two groups). Statistical significance of the *in vivo* experiment was assessed using Welch ANOVA and Games-Howell's test for multiple comparisons. Differences were considered statistically significant at $p < 0.05$. * , $p < 0.05$; * *, $p < 0.01$; * ** , $p < 0.001$; * ** *, $p < 0.0001$.

3. Results

3.1. Identification of three quinolines inhibiting the HH pathway downstream of SUFU

A virtual screening protocol comprising a pharmacophore-based ligand design approach and molecular docking simulations led us to identify three classes of negative modulators of GLI1 that were populated by thiophene, pyrazolo-pyrimidine, and quinoline derivatives [41, 42]. Structure-activity relationship considerations that emerged in previous studies prompted us to prioritize the 8-hydroxyquinoline SST0776

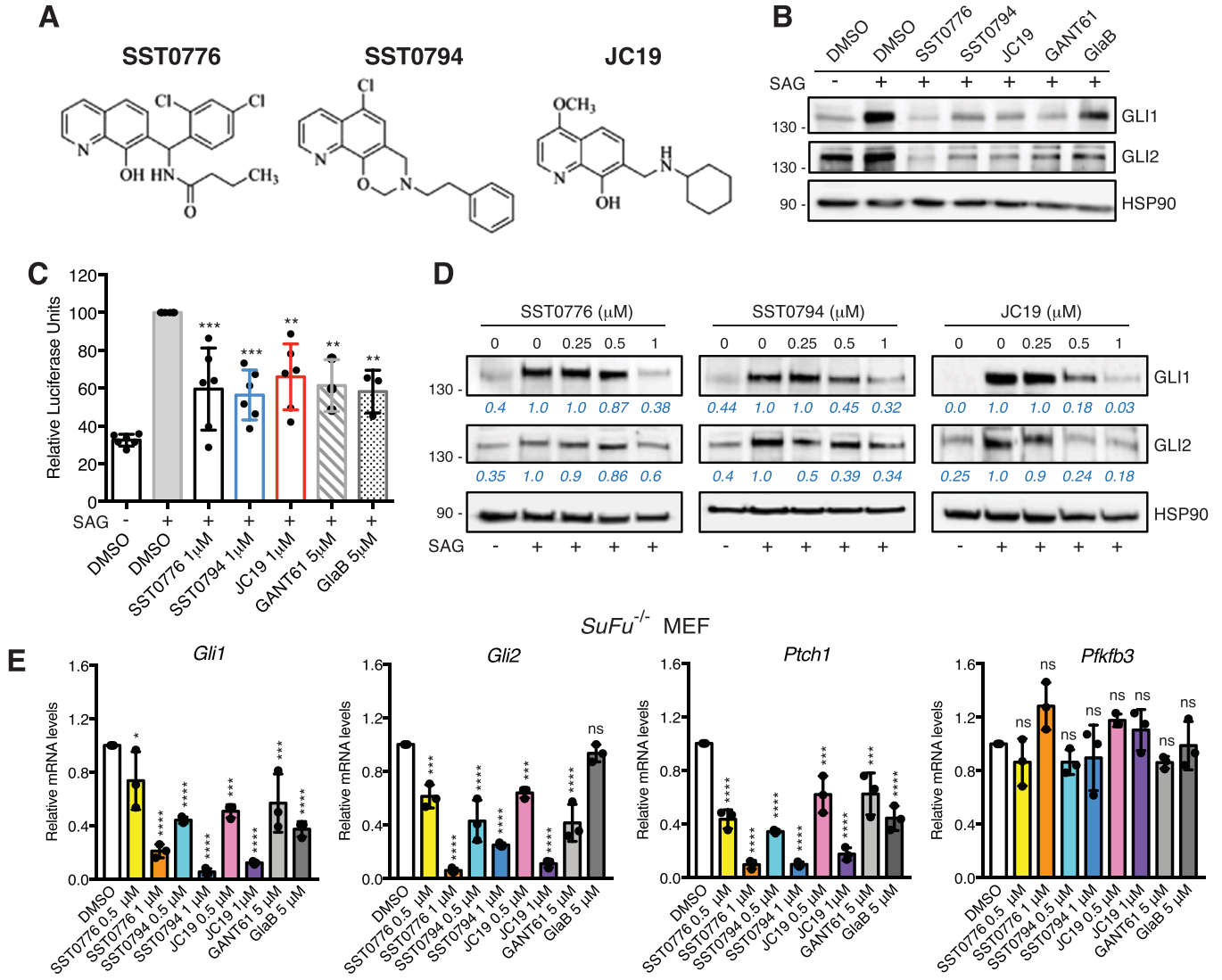

Fig. 1. The three quinolines inhibit endogenous HH pathway. A) Chemical structure of SST0776, SST0794, and JC19. B) Western blot of endogenous GLI1 and GLI2 in HH-responsive NIH3T3 cells stimulated with SAG (100 nM) and treated with SST0776, SST0794, and JC19 (1 μM) or the reference compounds GANT61 and GlaB (5 μM) for 48 h. HSP90 was used as loading control. C) Luciferase assay in NIH3T3 cells treated with SAG (100 nM) and SST0776, SST0794 and JC19 (1 μM) or the reference compounds GANT61 and GlaB (5 μM) for 48 h. Relative luciferase units were GLI-dependent reporter firefly/renilla control ratios, with cells treated with SAG equated to 100. D) Western blot of GLI1 and GLI2 in NIH3T3 cells treated with SAG (100 nM) and with increasing concentrations of SST0776, SST0794, and JC19 for 48 h. HSP90 was used as loading control. E) qPCR of *Gli1*, *Gli2*, *Ptch1,* and *Pfkfb3* in *SuFu*$^{-/-}$ MEFs treated with SST0776, SST0794, and JC19 at 0.5 and 1 μM, or GANT61 and GlaB at 5 μM for 48 h, with cells treated with DMSO equated to 1. Gene expression was normalized relative to *Gapdh* and *β2-microglobulin* (mean ± SD). * , $p < 0.05$; * *, $p < 0.01$; * ** , $p < 0.001$; * ** *, $p < 0.0001$, ns: not significant (one-way ANOVA). Data represent mean ± SD of at least three independent experiments.

and the oxazino-quinoline SST0794 for further biological evaluation as GLI inhibitors (Fig. 1A). Moreover, following a classical hit-to-lead optimization process by reducing the scaffold complexity of SST0794 and removing the chiral center of SST0776, we designed the simplified molecule JC19 (Fig. 1A), whose chemical synthesis and characterization are reported in the *SI Appendix* Materials and Methods. These three compounds were able to inhibit endogenous GLI1 and GLI2 protein levels and HH pathway transcriptional activity at 1 μM in NIH3T3 cells treated with the SMO agonist SAG [52]. Notably, these small molecules were more effective than the known GLI inhibitors GANT61 and GlaB, which were used at 5 μM (Fig. 1B and C). All three quinolines reduced GLI1 and GLI2 protein levels in a dose-dependent manner in NIH3T3 cells, with JC19 showing strong inhibition (80%) of GLI1 and GLI2 at 0.5 μM (Fig. 1D). The compounds strongly inhibited the expression of *Gli1, Gli2*, and several HH target genes in *Ptch1*$^{-/-}$ MEFs [53], in which GLI transcription factors are constitutively active (Supporting Fig. S1). To prove that these compounds act downstream of SMO, we used *SuFu*$^{-/-}$ MEFs, which harbor cell-autonomous activation of the HH pathway due to the genetic ablation of the negative regulator SuFu [54]. In these cells, the compounds reduced the expression of *Gli1, Gli2*, and *Ptch1* without affecting the unrelated gene *Pfkfb3* (Fig. 1E). Taken together, these findings indicate that SST0776, SST0794, and JC19 inhibit the endogenous HH pathway, acting downstream of SMO and SUFU.

3.2. SST0776, SST0794, and JC19 inhibit HH signaling by hampering GLI1 and GLI2 binding with the DNA

Treatment of HEK-293 T cells overexpressing GLI1 or GLI2 showed that SST0776 and SST0794 at the dose of 1 μM and JC19 at 2 μM slightly decreased expression of exogenous GLI1 or GLI2 (Supporting Fig. S2A). However, this reduction is proteasome independent, because treatment with the proteasome inhibitor MG132 did not revert this effect on GLI1 and GLI2 protein expression. (Supporting Fig. S2B and C). Therefore, to elucidate the mechanism of action of the three quinolines, we evaluated their effect on GLI1 and GLI2 transcriptional activity. Chromatin immunoprecipitation (ChIP) in HEK-293 T cells overexpressing GLI1 or GLI2 demonstrated that the quinolines inhibited HH signaling, impairing the binding of the GLI to DNA, as shown by the strong reduction in the recruitment of both GLI1 and GLI2 into the promoter of *PTCH1* (Fig. 2A-C). Consistently, the luciferase assay confirmed that all three quinolines inhibited the transcriptional activities of GLI1 and GLI2 in HEK-293 T cells overexpressing GLI1 or GLI2 (Fig. 2D and E). To further confirm that the three compounds inhibited transcriptional activity, HEK-293 T and A375 cells overexpressing GLI1 were treated with either SST0776, SST0794, or JC19 in presence of the G/C-specific DNA-binding drug mithramycin A to inhibit transcription. Quantitative PCR (qPCR) showed that mithramycin completely prevented the decrease in *PTCH1* mRNA levels induced by the three compounds (Fig. 2F and G). To further corroborate ChIP and luciferase results, we performed electrophoretic mobility shift assay (EMSA) and DNA pull-down assays in HEK-293 T cells expressing pBABE-GLI1 (EMSA) or Myc-tagged GLI1 (DNA pull-down) or empty vector. EMSA showed the binding of GLI1 to a GLI1 consensus DNA probe, which was strongly prevented by treatment of nuclear cell extracts with JC19. Pre-incubation of cell extracts with anti-GLI1 antibody decreased the formation of the complex, suggesting the presence of GLI1 protein (Fig. 2H). DNA pull-down experiments confirmed the strong inhibition of the formation of the GLI1/DNA complex in presence of JC19 (Fig. 2I), suggesting that JC19 competes with DNA for the DNA binding site of GLI1. Altogether, these findings suggest that JC19 inhibits transcriptional activity by impairing the binding of GLI1 and GLI2 to the DNA of the target genes.

3.3. Binding of JC19 to GLI1

Molecular docking calculations suggested that quinolines could be accommodated within two pockets of the GLI1 structure. In particular, one of the best scoring binding poses of JC19 (taken as a representative example of the quinoline derivatives (Fig. 2J) showed interactions similar to those previously hypothesized for thiophene and pyrazolo-pyrimidine compounds [41], as well as for GlaB [32]. The backbone and the imidazole NH groups of His351 (one of the amino acids that coordinate the zinc ion) formed hydrogen bonds with the quinoline nitrogen atom and with the C8 oxygen of the ligand. Additional hydrogen bonds were found between the basic protonatable amino nitrogen of JC19 and the side chain OH group of Thr374. Further complex stabilization was achieved through π-cation interactions between the aromatic quinoline and the terminal guanidine group of Arg354. Hydrophobic contacts were also found between the C4 methoxy group and the polymethylenic chain of Lys350. To support the hypothesis that these residues are important for the binding of JC19 to GLI1, the docked complex was used for the rational design of site-directed mutagenesis experiments on GLI1 structure. Amino acids directly involved in the interactions with JC19 (His351, Arg354, and Thr374) or belonging to its binding pocket on GLI1 (Thr355 and His356) were prioritized for mutation. Substitutions of these residues by Ala were expected to change the structural features of the binding pocket, thus reducing or preventing the interactions of JC19 with GLI1, with a consequent decrease of JC19 ability to reduce GLI1 transcriptional activity.

Mutagenesis studies showed that the residues belonging to ZF4 and ZF5 are involved in GLI1 binding to DNA. Luciferase assay in HEK-293 T cells transiently transfected with GLI1 or GLI1 mutants indicated that mutations in H351 and R354 almost completely abrogated GLI1 transcriptional activity, H356 and T374 reduced it respectively by 50% and 40%, and T355 did not affect it (Fig. 2K). Notably, H351A and, to a lesser extent, H356A mutants reduced the ability of JC19 to inhibit GLI1 transcriptional activity (Fig. 2L), suggesting that JC19 interacts with GLI1 at the level of H351 and H356 residues.

3.4. The three quinolines inhibit GLI-dependent growth of several cancer cell types

To address the ability of our compounds to reduce cancer cell proliferation, we investigated whether these small molecules could inhibit the GLI-dependent growth of human cancer cells with GLI1 and GLI2 activation. Treatment of a panel of commercial (A375, MeWo, and SK-Mel-5) and primary (SSM2c and Me-53) melanoma cells, glioblastoma (U87-MG), medulloblastoma (DAOY), breast cancer (MCF7), and intrahepatic cholangiocarcinoma cell lines (HuCCT1, CCLP1) with the three compounds for 72 h resulted in a dose-dependent reduction of cancer cell growth, with IC_{50} ranging from 0.1 μM to 1.6 μM (Figs. 3A and 3B; Supporting Fig. S3). In contrast, treatment of normal human epidermal melanocytes (NHEM) and non-neoplastic mammary epithelial cell line (MCF10A) with SST0776, SST0794, and JC19 had effects on cell viability only at the highest concentrations (5 and 10 μM). Among them, JC19 showed the highest IC_{50} in NHEM and MCF10A, indicating that JC19 is more effective in cancer cells than in non-neoplastic cells (Fig. 3B; Supporting Fig. S3). NHEM and MCF10A cells expressed the lowest levels of *GLI1* and *GLI2* mRNA, whereas DAOY cells showed the highest levels of *GLI1* and *GLI2*, and the lowest IC_{50} (Fig. 3B; Supporting Fig. S3 and S4). Treatment of A375, MeWo, SK-Mel-5, and U87-MG cells with the three compounds for 24 or 48 h significantly reduced the levels of *GLI1, GLI2*, and *PTCH1* in a dose-dependent manner (Fig. 3C-E; Supporting Fig. S5). Altogether, these findings indicate that all the compounds strongly reduced GLI-dependent cancer cell growth.

Inhibition of the HH signaling pathway has been reported to increase apoptotic cell death [26,55]. Therefore, we investigated whether the three quinolines inhibited cancer cell growth by affecting apoptosis. Treatment of A375, MeWo, SK-MEL-5, and U87-MG cells with SST0776, SST0794, and JC19 led to a dose-dependent increase in both early and late apoptosis, as shown by Annexin V/7-AAD staining (Fig. 4A-C; Supporting Fig. S6 and 7). Induction of apoptosis was confirmed for JC19 at the molecular level by an enhanced BAX/BCL-2 ratio and

increased cleaved caspases 3 and 9 (Figs. 4D and 4E). In addition, treatment with JC19 induced a dose-dependent increase of caspase 3/7 activities (Fig. 4F).

3.5. Specificity for GLI1 and GLI2

To assess the specificity of our molecules for GLI1 and GLI2, we silenced GLI1 and GLI2 using specific shRNAs [43,44] in U87-MG and MeWo cells, which express moderate levels of GLI1 and GLI2 (Supporting Fig. S4). Silencing of GLI1 and/or GLI2 resulted in a drastic reduction in GLI1 and GLI2 mRNA and protein levels in both cell lines (Figs. 5A and 5B). Importantly, silencing of GLI1 or GLI2 made cells less sensitive to growth inhibition induced by treatment with SST0776, SST0794, or JC19 (Figs. 5C and 5D), as previously demonstrated with other GLI-targeting small molecules [32,41]. Moreover, in GLI1- and GLI2-silenced cells the ability of the three molecules to repress *PTCH1* mRNA levels was completely abrogated (Fig. 5E). To further address the specificity for GLI1, we knocked it down in U87-MG cells using

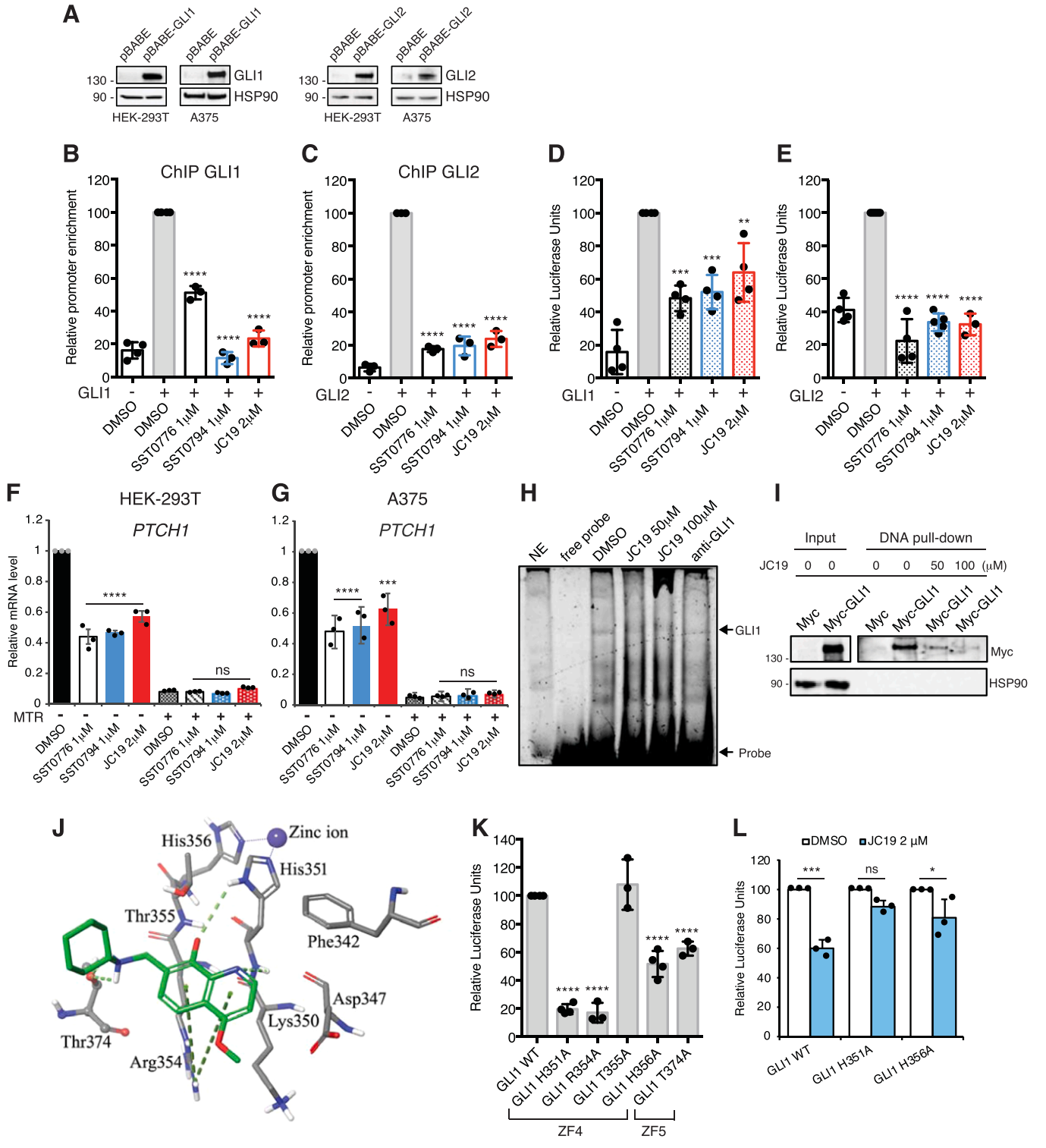

(caption on next page)

Fig. 2. The three quinolines inhibit HH signaling by impairing the binding of GLI1 and GLI2 to DNA. A) Western blot of GLI1 and GLI2 in HEK-293 T and A375 cells transduced with pBABE, pBABE-GLI1 or pBABE-GLI2. HSP90 was used as loading control. B-C) Chromatin immunoprecipitation (ChIP) of GLI1 (B) and GLI2 (C) in HEK-293 T transduced with pBABE, pBABE-GLI1 or pBABE-GLI2, and treated with SST0776 (1 μM), SST0794 (1 μM), and JC19 (2 μM) for 16 h. Relative promoter enrichment of *PTCH1* was normalized on the input material. Cells transduced with pBABE-GLI1 or pBABE-GLI2 and treated with DMSO were equated to 100. D-E) Luciferase assay in HEK-293 T cells transduced with pBABE, pBABE-GLI1 or pBABE-GLI2 and treated with SST0776 (1 μM), SST0794 (1 μM), and JC19 (2 μM) for 16 h. Relative luciferase units were GLI-dependent reporter firefly/renilla control ratios, with cells overexpressing GLI1 or GLI2 and treated with vehicle (DMSO) equated to 100. F-G) qPCR of *PTCH1* in HEK-293 T and A375 transduced with pBABE-GLI1 and treated with Mithramycin A (MTR) (200 nM) and the three compounds as indicated for 16 h. Cells overexpressing GLI1 and treated with DMSO were equated to 1. Gene expression was normalized relative to *GAPDH* and *TBP* and expressed as mean ± SD. H) Inhibition of GLI1/DNA binding by JC19. EMSA using 20 μg of nuclear extract (NE) obtained from HEK-293 T cells overexpressing GLI1 and incubated with double-stranded oligonucleotide containing the GLI binding site sequence (probe) in presence of JC19 (50 and 100 μM) or the anti-GLI1 antibody. The arrows represent free probe and probe bound to GLI1. I) SDS-PAGE of DNA pull-down assay. 150 μg of whole cell lysate (WCL) obtained from HEK-293 T cells overexpressing Myc-GLI1 or Myc-Empty vector as control were incubated with the GLI binding site 3'- biotinylated probe in the presence of JC19 (50 and 100 μM). 10 μg of WCL from cells containing Myc-GLI1 or Myc-Empty vector were loaded as input proteins. HSP90 was used as loading control. J) Graphical representation of the best docked binding poses of JC19 (thick line, carbon custom color and atom type notation) within the GLI1 binding site also hypothesized for thiophene and pyrazolo-pyrimidine derivatives, as well as for GlaB. For the sake of clarity, only a few amino acids are shown (thick lines, atom type notation with labels and grey surface). Hydrogen bonds are represented by light green dashed lines, while cation-π interactions by green dashed lines. K) Luciferase assay in HEK-293 T cells transfected with GLI1 WT or indicated GLI1 mutants in ZF4 and ZF5. Relative luciferase units were GLI-dependent reporter firefly/renilla control ratios, with cells overexpressing GLI1 WT equated to 100. L) Luciferase assay in HEK-293 T cells transfected with GLI1 WT, GLI1 H351A or GLI1 H356A and treated with JC19 (2 μM) for 16 h. Relative luciferase units were GLI-dependent reporter firefly/renilla control ratios. Cells treated with DMSO were equated to 100. * , $p < 0.05$; * *, $p < 0.01$; * ** , $p < 0.001$; * ** *, $p < 0.0001$, ns: not significant (one-way ANOVA). Data represent mean ± SD of at least three independent experiments.

CRISPR/Cas9. Consistent with the results obtained from the genetic silencing, the three compounds showed minor effects in reducing cancer cell viability in the GLI1-ko bulk population compared to control cells transduced with scrambled sgRNA (Figs. 5F and 5G). Taken together, these findings indicate that both GLI1 and GLI2 are required for the anti-tumor activity of the three quinolines.

To verify that the observed activity was not due to off-target effects, the catalytic activity of a panel of 77 protein kinases related to the HH pathway or known to modulate GLI activity [56], was tested in the presence of JC19. The *in vitro* enzymatic assay showed that 10 μM JC19 did not significantly affect the activity of these kinases (Supporting Fig. S8). Because Jun/AP-1 has been reported to synergize with GLI1 [57], we tested the effect of our compounds on this target, finding that they did not alter the expression of *cJUN* in U87-MG and MeWo cells (Supporting Fig. S9). In addition, JC19 treatment did not affect GLI3 protein levels (Supporting Fig. S10A). To further confirm the specificity of JC19 for GLI1 and GLI2, we tested whether JC19 treatment inhibits other related GLI-similar transcription factors or the C2H2 ZIC factors. Western blot and qPCR analysis showed that the expression levels of ZIC1, ZIC2, ZIC3, GLIS1, GLIS2, GLIS3, and of the specific ZIC transcription factor target Apolipoprotein E are not affected by JC19 (Supporting Fig. S10B-F).

3.6. ADME and PK parameters

To identify a potential lead compound among our molecules, the ADME profiles of these three compounds were investigated (Fig. 6A). JC19 was characterized by the highest aqueous solubility (813.62 μg/mL corresponding to a logS = −2.56), while SST0776 and SST0794 resulted much less soluble with solubility values of 0.52 μg/mL (logS of −5.87) and 2.95 μg/mL (logS of −5.04), respectively. The solubility of JC19 was also tested in HEPES buffer (25 mM, NaCl 140 mM, pH 7.4) confirming the trend (741.23 μg/mL, logS −2.59). All three quinolines were characterized by high plasma stability (98% after 24 h incubation with human plasma). The PAMPA assay was also performed to establish the ability of the compounds to cross cellular membranes and simulate intestinal absorption for passive diffusion. All of them were highly permeable, with permeability values of 12.16, 12.98, and 15.35 × 10^{-6} cm/sec for SST0776, JC19, and SST0794, respectively. Furthermore, the percentage of membrane retention was calculated for all compounds, highlighting a nonrelevant interaction with the phospholipidic bilayer. Finally, stability in the presence of HLMs was investigated, suggesting that derivatives were all able to overcome the metabolic process without undergoing significant structural modifications (values > 95%). Although all quinolines showed excellent plasma and metabolic stability and high passive permeability, JC19 was selected for the *in vivo* studies because of its high aqueous solubility, which ensures a good bioavailability to a potential future oral administration.

The plasmatic concentration-time curves and the PK parameters revealed that JC19 was characterized by a first-order elimination kinetics, as shown by the logarithmic curve (Fig. 6B). After the intraperitoneal (i.p.) administration, JC19 reached the C_{max} (0.890 and 1.570 μg/mL for the lower and higher dosages, respectively) in at least 5 min (T_{max} 0.083 h), but the rapid kinetics of elimination were confirmed by the low half-life ($t_{1/2}$), the MRT values, and the high clearance (CL) values (Fig. 6C). The rapid elimination rate of JC19 from the body can be also appreciated from the tissue biodistribution (BD) profiles (Fig. 6B). After the i.p. administration, a low accumulation of JC19 was also observed in the liver (Fig. 6D). JC19 was then subjected to an additional assay to study its binding to human serum albumin (HSA) using the C_{max} obtained after its *in vivo* administration at 25 mg/kg. The results obtained by incubating JC19 with HSA show that the molecule does not bind the protein, with a percentage of unbound compound of 99.9%. This value reflects the hydrophilic profile of JC19 already shown with the aqueous solubility, and it makes the compound available to reach the target and carry out its antitumor activity. Based on the results described above, JC19 was selected as the lead compound for further *in vivo* evaluation in a human melanoma xenograft model.

3.7. JC19 treatment reduces human melanoma xenograft growth in vivo

To address the ability of JC19 to inhibit GLI function and subsequent tumor growth *in vivo*, we used a human orthotopic xenograft model of melanoma. Athymic nude mice were subcutaneously injected with A375 melanoma cells, which harbor both canonical and noncanonical HH pathway activation and are sensitive to SMO and GLI inhibition [24,26,41,43]. Moreover, these cells show the lowest IC_{50} value for JC19 together with HH-dependent DAOY medulloblastoma cells (Fig. 3A and B; Supporting Figs. S3 and 4). When tumors were palpable (approximately 20 mm^3), mice were randomized into three groups and treated for 12 days with i.p. injection of JC19 at 15 mg/kg, 25 mg/kg, or vehicle alone (10% DMSO in PBS) (Fig. 6E). Based on PK parameters showing rapid elimination kinetics, the mice were treated with JC19 twice a day. Administration of JC19 at 15 mg/kg and, to a greater extent, at 25 mg/kg produced a significant decrease in tumor growth compared with vehicle-treated mice (Figs. 6F and 6G). Although the plasma concentration of JC19 dropped rapidly after administration, an effective dose for tumor growth reduction was reached. During the 12-day of JC19 treatment, we did not observe adverse side effects, such as weight loss (Fig. 6H), tumor ulcerations, or general unhealthiness of the mice, indicating good tolerance of JC19. qPCR analysis of the status of HH pathway activation in xenografted tumors revealed that administration

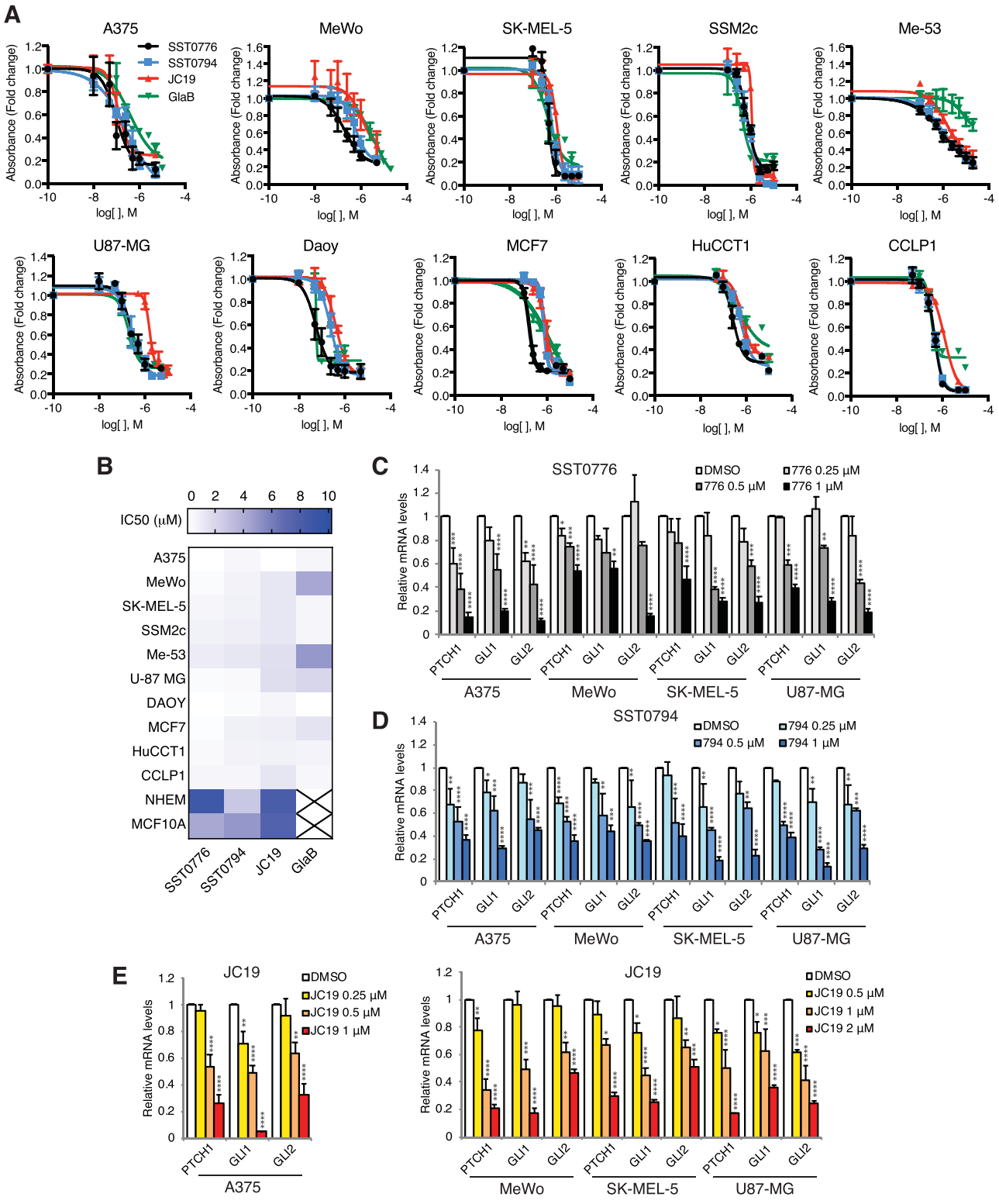

Fig. 3. SST0776, SST0794 and JC19 repress proliferation of multiple cancer cell lines through inhibition of GLI-mediated transcription. A) Dose response curves of commercial (A375, MeWo, and SK-MEL-5) and primary (SSM2c and Me-53) melanoma, U87-MG glioblastoma, Daoy medulloblastoma, MCF7 breast cancer, HuCCT1 and CCLP1 cholangiocarcinoma cells. Cells were treated for 72 h with vehicle (DMSO) or increasing doses of compounds and GlaB. Graphs were obtained using GraphPad 7. B) Heatmap of IC_{50} values in cancer cells shown in A, normal human epidermal melanocytes (NHEM) and mammary epithelial breast cells (MCF10A) treated with increasing doses of SST0776, SST0794, and JC19 for 72 h. C-E) qPCR of *PTCH1*, *GLI1,* and *GLI2* in A375, MeWo, SK-MEL-5, and U87-MG cells treated with increasing concentrations of SST0776 (C), SST0794 (D), and JC19 (E) for 24 h with cells treated with DMSO equated to 1. Gene expression was normalized relative to *GAPDH* and *TBP* and expressed as mean ± SD. * , $p < 0.05$; * *, $p < 0.01$; * ** , $p < 0.001$; * ** *, $p < 0.0001$, ns: not significant (one-way ANOVA). Data represent mean ± SD of at least three independent experiments.

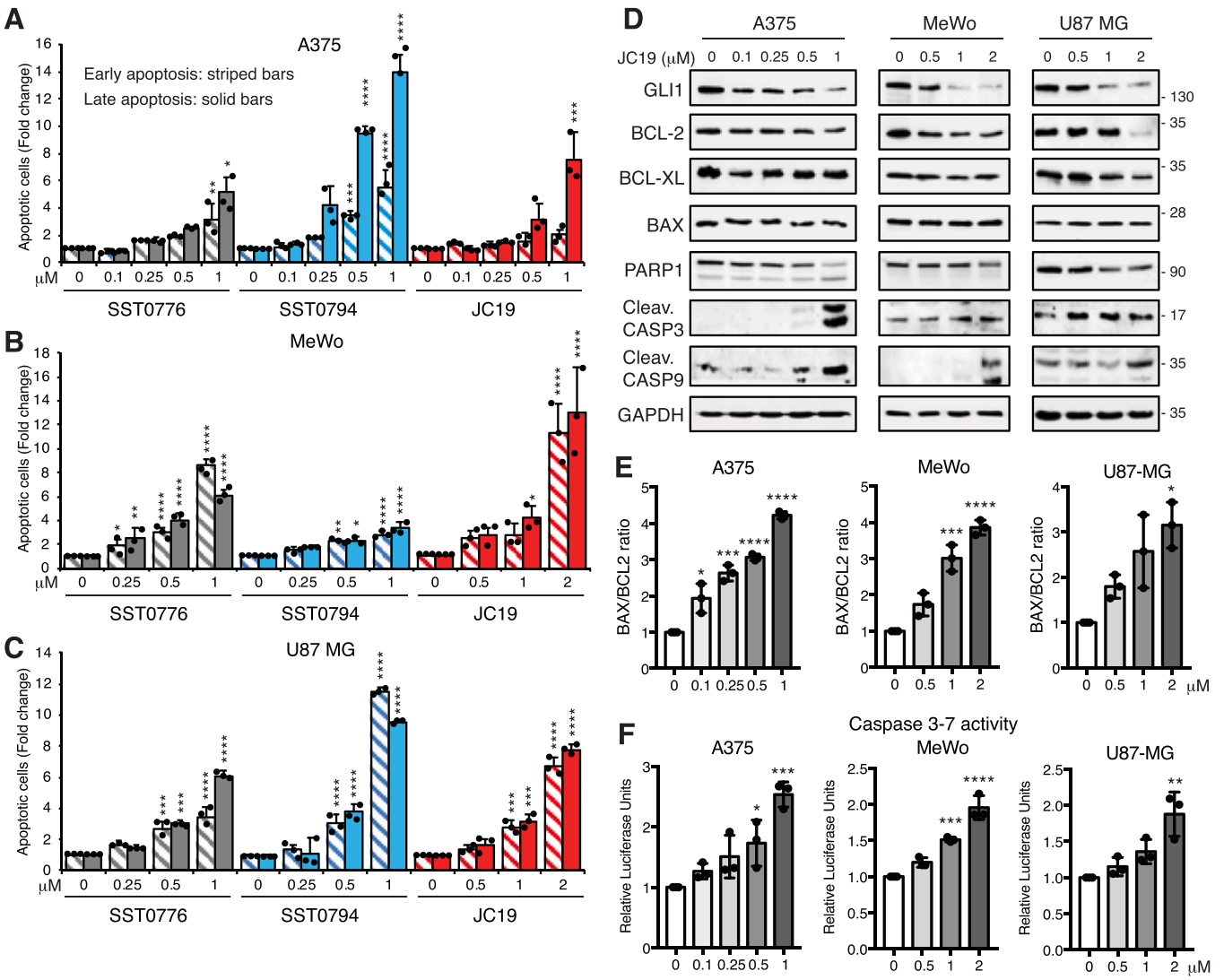

Fig. 4. GLI inhibition induces apoptosis in cancer cells. A-C) AnnexinV/7-AAD double staining of early (AnnexinV+/7-AAD-) and late (AnnexinV+/7-AAD+) apoptosis of A375 (A), MeWo (B), and U87-MG (C) cells treated with increasing doses of SST0776, SST0794, and JC19 for 72 h, with cells treated with DMSO equated to 1. D) Western blot of GLI1, BCL-2, BCL-XL, BAX, PARP1, cleaved Caspases 3 and 9 in A375, MeWo, and U87-MG cells treated with increasing doses of JC19 for 72 h. GAPDH was used as loading control. E) Densitometric quantification of BAX/BCL-2 ratio as shown in D. F) Activity of Caspase 3 and 7 in A375, MeWo and U87 cell lines treated with increasing doses of JC19 for 72 h. Cells treated with DMSO were equated to 1. * , $p < 0.05$; * *, $p < 0.01$; * ** , $p < 0.001$; * ** *, $p < 0.0001$ (one-way ANOVA). Data represent mean ± SD of at least three independent experiments.

of JC19 for 72 h significantly reduced the expression level of *GLI1* in a dose-dependent manner compared to vehicle alone (Fig. 6I), in line with the *in vitro* data (Fig. 3C-E). Taken together, these findings suggest that JC19 administration impairs GLI-dependent tumor growth *in vivo* in a dose-dependent manner.

4. Discussion

In this study, we discovered three small molecules (two 8-hydroxyquinolines SST0776 and JC19, and the oxazino-quinoline SST0794) capable of inhibiting GLI1 and GLI2 activities. Pharmacological inhibition of GLI1 and GLI2 resulted in a dose-dependent anti-tumor response in multiple cancer cell lines *in vitro* and reduction of tumor growth in a melanoma xenograft model *in vivo*.

In recent years HH signaling has emerged as an attractive target for anti-cancer therapy. Several inhibitors of the key transducer SMO have been developed and are available for the treatment of advanced BCC [5, 58]. However, SMO inhibitors have several limitations. First, SMO undergoes several mutations that can render cancer cells resistant to pharmacological inhibition of SMO [59,60]. Second, these inhibitors are not effective in tumors harboring noncanonical activation of the HH pathway, such as those with inactivating mutations of *SUFU* or amplification of *GLI1* and *GLI2* genes. In addition, several types of cancer present noncanonical activation of the GLI transcription factors by other oncogenic signals and inputs that can be independent of upstream PTCH-SMO [17]. Therefore, targeting the GLI transcription factors can inhibit both canonical and noncanonical HH activation, thereby blocking the final effectors of the pathway. To date, only a few specific GLI inhibitors have been developed, such as GANT61 [31], and GlaB [32]. However, these molecules suffer from poor drug-like properties, such as low solubility, poor metabolic stability, and modest activity, with high concentrations required for the inhibition of the target *in vitro* and tumor growth *in vivo*.

Another recent virtual screening study identified an 8-hydroxyquinoline as a GLI1 negative modulator [61]. Authors showed that this molecule inhibits GLI1-mediated transcription, likely causing conformational changes in the GLI1/DNA complex, without providing a clear mechanism for GLI1 inhibition. Moreover, the activity of this compound

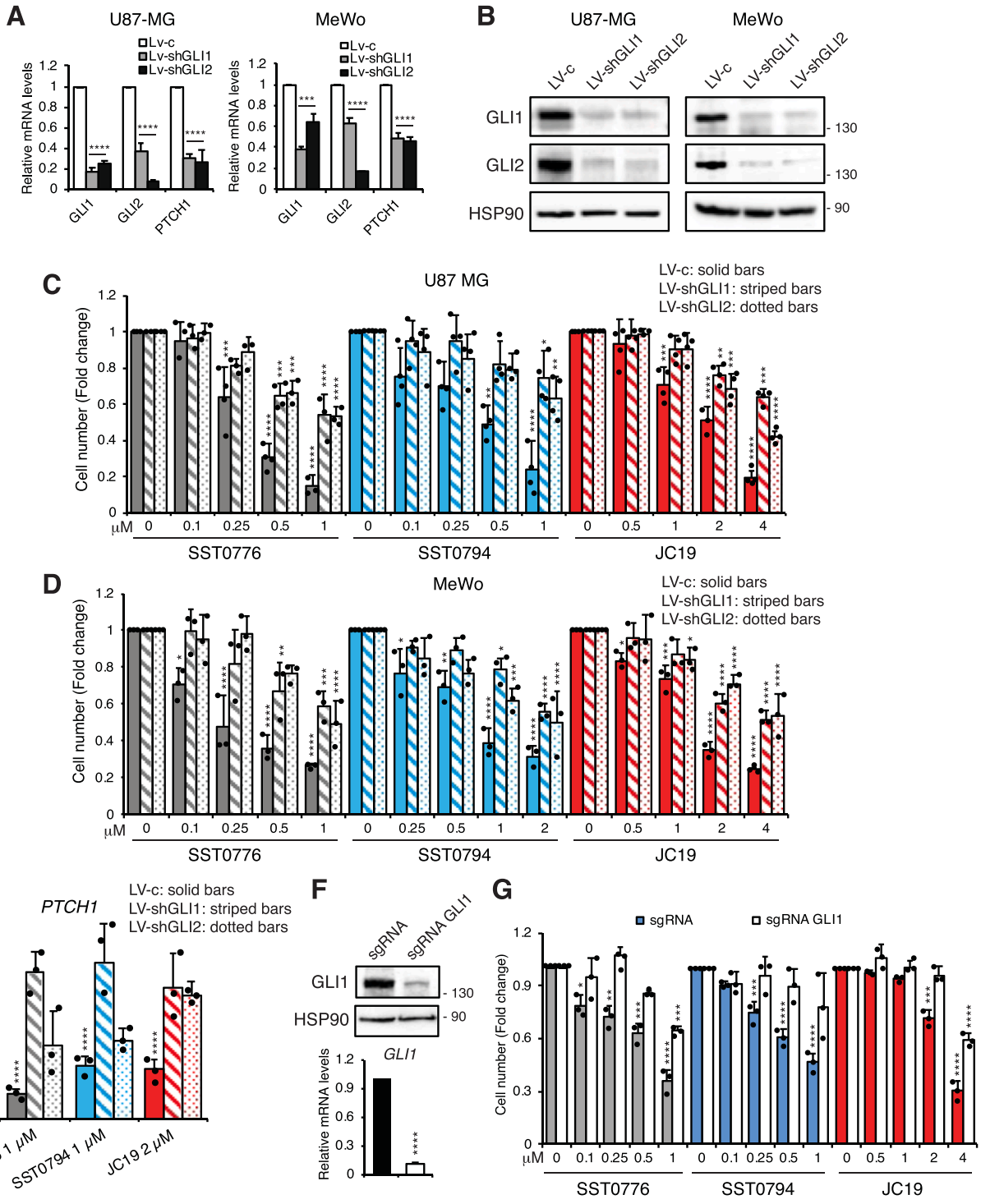

Fig. 5. GLI1 and GLI2 are required for inhibition of cell proliferation and transcriptional activity by the three quinolines. A) qPCR of *GLI1*, *GLI2* and *PTCH1* in U87-MG and MeWo cells transduced with LV-c, LV-shGLI1 or LV-shGLI2, with cells transduced with LV-c equated to 1. Gene expression was normalized relative to *GAPDH* and *TBP* and expressed as mean ± SD. B) Western blot of GLI1 and GLI2 in U87-MG and MeWo cells transduced with LV-c, LV-shGLI1 or LV-shGLI2. HSP90 was used as loading control. C-D) Growth curves of U87-MG and MeWo cells transduced with LV-c, LV-shGLI1 or LV-shGLI2 and treated with increasing doses of SST0776, SST0794, and JC19 for 72 h. Cells treated with DMSO were equated to 1. E) qPCR of *PTCH1* in U87-MG cells transduced with LV-c, LV-shGLI1 or LV-shGLI2, and treated with SST0776 (1 μM), SST0794 (1 μM), and JC19 (2 μM) for 24 h. Cells treated with DMSO were equated to 1. F) Western blot (upper panel) and qPCR (lower panel) of GLI1 in U87-MG cells transduced with pCW-Cas9 and sgRNA (scrambled) or sgRNA GLI1. G) Growth curves of U87-MG cells transduced with pCW-Cas9 and sgRNA (scrambled) or sgRNA GLI1, and treated with increasing concentrations of SST0776, SST0794, and JC19 for 72 h, with cells treated with DMSO equated to 1. * , $p < 0.05$; * *, $p < 0.01$; * ** , $p < 0.001$; * ** *, $p < 0.0001$ (one-way ANOVA). Data represent mean ± SD of at least three independent experiments.

A

Cmpd	Aqueous Solubility (μg/mL)		Plasma Stability[b] (%)	PAMPA (10^{-6}cm/sec) (%MR[c])	Metabolic Stability (%)[d] ± SD
	H_2O MilliQ	Buffer Solution[a]			
SST0776	0.52 (logS = -5.87)	–	> 98	12.16 (9.59)	98.30 ± 0.07
SST0794	2.95 (logS = -5.04)	–	> 98	15.35 (21.57)	95.69 ± 0.35
JC19	813.62 (logS = -2.56)	741.23 (logS = -2.59)	> 98	12.98 (17.28)	99.35 ± 0.09

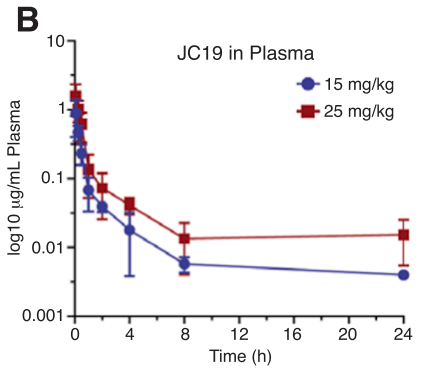

C

JC19 PK Parameters

Parameters	Unit	15 mg/kg	25 mg/kg
$t_{1/2}$	h	6.479	4.353
T_{max}	h	0.083	0.083
C_{max}	μg/mL	0.890	1.570
$AUC_{0\text{-}24h}$	μg/mL*h	0.548	1.228
$AUC_{0\text{-}inf}$	μg/mL*h	0.586	1.324
$MRT_{0\text{-}inf}$	h	5.004	5.983
Vz/F	(mg/kg)/(μg/mL)	239.142	118.518
Cl/F	(mg/kg)/(μg/mL)/h	25.583	18.869

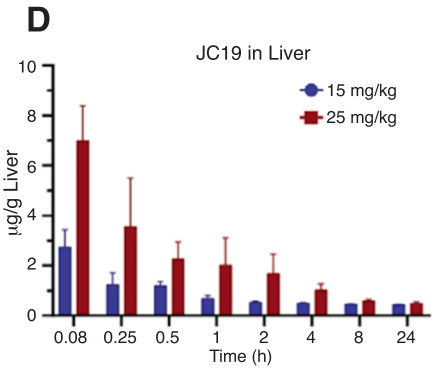

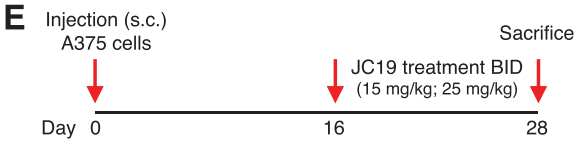

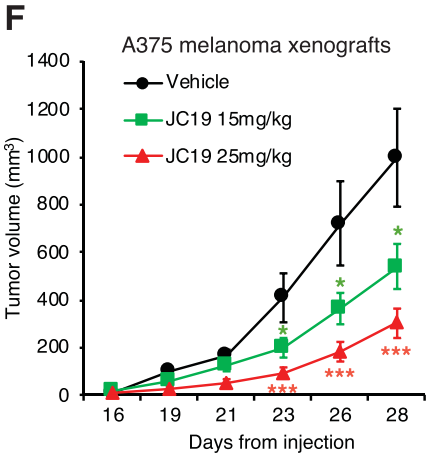

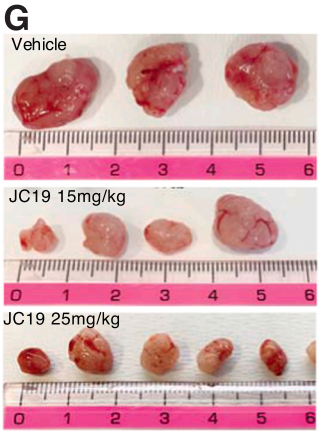

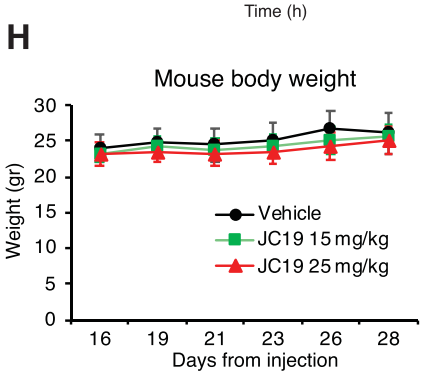

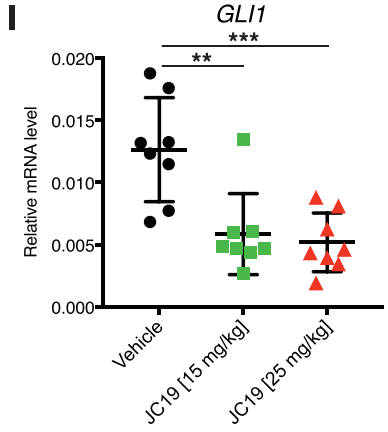

Fig. 6. JC19 ADME, PK parameters and growth inhibition in melanoma xenografts. A) Table shows ADME parameters for the three quinolines. [a]Buffer solution: HEPES 25 mM, NaCl 140 mM, pH 7.4. [b]After 24 h incubation in human plasma solution. [c]Membrane Retention (%MR) expressed as percentage of compound unable to reach the acceptor compartment. [d]Expressed as percentage of unmodified compound. B) Plasma concentration-time curves (mean ± SD, n = 6) after intraperitoneal administration of JC19 15 mg/kg and 25 mg/kg. The plasma concentrations in the y axis were expressed as $\log_{10}$ scale. C) Table shows pharmacokinetics parameters of JC19 after i.p. administration evaluated using a non-compartmental model. D) Liver distribution concentration profile (mean ± SD, n = 6) of JC19 at the dosages of 15 and 25 mg/kg. E) Experiment timeline of the *in vivo* treatment. F) *In vivo* growth of A375 melanoma cells subcutaneously injected in athymic nude mice. Mice were treated i.p. at tumor appearance with vehicle, JC19 15 mg/kg or 25 mg/kg twice a day. G) Representative images of tumors at the sacrifice. H) Mice body weight during treatment. I) qPCR of *GLI1* in melanoma xenografts treated with vehicle, JC19 15 mg/kg or 25 mg/kg for 72 h. Gene expression was normalized relative to *GAPDH* and *TBP* and expressed as mean ± SEM. * , $p < 0.05$; * *, $p < 0.01$; * ** , $p < 0.001$ (one-way ANOVA).

appeared very modest, with a dose of 25 μM required for the inhibition of GLI1 and GLI2 protein levels. Finally, the specificity of this 8-hydroxyquinoline for GLI1 and/or GLI2 has not been addressed. Therefore, there is a need to identify new small molecules that target GLI transcription factors.

Recently, a virtual screening approach allowed us to identify several small molecules capable of inhibiting HH-dependent transcription, as well as GLI1 and GLI2 protein levels. Most of the compounds identified by the virtual screening were confirmed to be GLI inhibitors [41,42]. Two of them (namely, SST0776 and SST0794) showed a strong reduction in GLI1 protein levels and were characterized by antiproliferative activity toward both human melanoma and medulloblastoma cell lines in the sub-micromolar range. Next, a hit-to-lead process based on the structural simplification of their molecular scaffold led to the design and synthesis of JC19.

Exploring the mechanism of inhibition, we found that despite their structural differences, the three quinolines identified in this study inhibited GLI-mediated transcription, impairing the binding of GLI1 and GLI2 to the DNA of target genes, as shown by the reduced occupancy of GLI1 and GLI2 on the *PTCH1* promoter. Furthermore, mithramycin treatment completely abrogated the effects of these molecules in reducing *PTCH1* mRNA levels. As a consequence, all three compounds strongly repressed the expression of several HH target genes in a broad spectrum of cancer cell lines. In addition, EMSA and DNA pull-down experiments demonstrated that JC19 inhibits the formation of GLI1/DNA complex. The interference of JC19 with the GLI1 DNA complex is further supported by our molecular docking study, suggesting that JC19 interacts with GLI1, likely making contacts with amino acids located in ZF4 and ZF5. Indeed, site-directed mutagenesis pointed out that residue H351, which is located in ZF4 and coordinates the zinc ion, is involved in the interaction of GLI1 with JC19. Targeting the interaction of GLI1 and GLI2 with DNA represents a successful strategy to block both PTCH/SMO-dependent (canonical) and noncanonical activation of the HH pathway, blunting the oncogenic hyperactivation of the signaling cascade.

Another important aspect of this study is that we provide evidence that knock-down of GLI1 or GLI2 by genetic silencing or CRISPR/Cas9 highly reduces the effects of our compounds on cancer cell proliferation and HH target genes expression. The residual inhibitory activity on cancer cell proliferation observed upon ablation of either GLI1 or GLI2 might be due to the ability of GLI1 to compensate for the loss of GLI2 and *vice versa* [62]. Our attempt to deplete both GLI1 and GLI2 was not successful, because cancer cells lacking both TFs were not viable, making impossible to test the effects of these quinolines on double GLI1 and GLI2 knock-down cells. The specificity of our compounds for GLI1 and GLI2 was further corroborated by the lack of effect of JC19 on the catalytic activity of a panel of 77 protein kinases related to the HH pathway or reported to modulate the function of GLI transcription factors through post-translational modifications. Furthermore, JC19 treatment does not affect GLI3 protein levels, or related GLI-similar TFs and other C2H2 zinc-finger TFs such as GLIS1, GLIS2, GLIS3, ZIC1, ZIC2 and ZIC3.

A preliminary *in vitro* ADME profile prompted us to select JC19 as the lead compound and test its anti-cancer activity *in vivo*. Unlike SST0776 and SST0794, JC19 showed a good aqueous solubility (approximately 1 mg/mL). Although PK analysis showed that after a single i.p. administration JC19 was characterized by a low half-life and high clearance, its administration twice a day for 12 days resulted in a dose-dependent inhibition of tumor growth, reaching a 70% reduction in tumor volume at a dose of 25 mg/kg. Notably, the mice did not show any signs of systemic toxicity during treatment and JC19 did not accumulate in the liver after the i.p. administration.

As a biomarker of response, we evaluated the expression level of *GLI1*, which is not only the main target of JC19, but also the best readout of the HH pathway activation. Administration of JC19 twice a day for 72 h reduced *GLI1* mRNA levels in a dose-dependent manner in melanoma xenografts compared to vehicle treated tumors.

In the context of melanoma, JC19 treatment might also contribute to prevent resistance to BRAF inhibitors, because targeting GLI1 and GLI2 with GANT61 has been shown to restore sensitivity to vemurafenib-resistant human melanoma cells [63]. In addition, aberrant activation of HH pathway has been shown to promote escape of cancer cells from immune surveillance by inducing the expression of programmed death ligand 1 (PD-L1) in several human cancer types [64]. Likewise, GANT61 treatment reduces PD-L1 expression and cancer cell proliferation in gastric cancer organoids [65]. Therefore, inhibition of GLI1 and GLI2 holds a great potential to elicit a robust anti-tumor immune response against cancer cells [66]. At this regard, treatment of BCC patients with the SMO inhibitor vismodegib was reported to produce an anti-cancer immune response, characterized by increased levels of MHC-I expression in cancer cells and infiltration of anti-tumor cytotoxic CD8+ and CD4+ T cells [67].

In summary, we describe the hit-to-lead design and synthesis of the new quinoline derivative JC19 and the biological characterization of three potent small molecules active as inhibitors of GLI. In particular, the lead compound JC19 showed the potential to inhibit GLI1 and GLI2 hyperactivation induced not only by upstream PTCH/SMO-dependent signals, but also by bypass mechanisms induced by oncogenic inputs.

5. Conclusion

GLI transcription factors, the final effectors of the Hedgehog signaling, are emerging as promising therapeutic targets for several human cancers. However, only a few GLI inhibitors are available. Here, we present the development and preclinical characterization of three novel small molecule GLI inhibitors that can suppress cancer cell proliferation and impair GLI1 and GLI2 activities by interfering with their binding to DNA. Among them, JC19 inhibits GLI-dependent human melanoma xenograft growth *in vivo*, with no signs of toxicity in mice. Our results highlight the potential therapeutic value of JC19 as an anti-tumor agent targeting GLI transcription factors, providing a rationale for testing JC19 in a broad spectrum of tumors with hyperactivation of GLI1 and GLI2.

Author Contribution

B.S., M.T., E.P., F.Manetti, G.G. designed research. L.M., E.C., F. Migliorini, G.A., A.G., S.P., F.P., C.V., A.L., E.P., B.S. performed research. L.M., E.C., G.A., F.P., C.V., A.L., E.D., B.S. analyzed data. F.Manetti performed virtual screening and molecular docking analysis. S.S. and L. B. contributed patient samples. L.M., E.P., F.Manetti and B.S. wrote the paper.

CRediT authorship contribution statement

Luisa Maresca: Data curation, Formal analysis, Investigation, Methodology, Writing original draft, Review & editing. Enrica Crivaro: Formal analysis, Investigation, Methodology, Review & editing. Francesca Migliorini: Investigation, Methodology, Review & editing. Giulia Anichini: Investigation, Review & editing. Alessandro Giammona: Investigation, Review & editing. Sara Pepe: Investigation, Review & editing. Federica Poggialini: Formal analysis, Investigation, Review & editing. Chiara Vagaggini: Formal analysis, Investigation, Review & editing. Giuseppe Giannini: Conceptualization, Review & editing. Serena Sestini: Resources, Review & editing. Lorenzo Borgognoni: Funding acquisition, Resources, Review & editing. Andrea Lapucci: Methodology, Review & editing. Elena Dreassi: Formal analysis, Writing original draft, Review & editing. Maurizio Taddei: Conceptualization, Funding acquisition, Review & editing. Fabrizio Manetti: Conceptualization, Software, Writing original draft, Review & editing. Elena Petricci: Conceptualization, Methodology, Funding acquisition, Writing original draft, Review & editing. Barbara Stecca: Conceptualization, Formal

analysis, Investigation, Project administration, Visualization, Funding acquisition, Supervision, Writing original draft, Review & editing.

Declaration of Competing Interest

The authors declare that they have no known competing financial interests or personal relationships that could have appeared to influence the work reported in this paper.

Data Availability

Data will be made available on request.

Acknowledgments

This work was supported by Bando Ricerca Salute 2018 (GLI SELTHER) (B.S., M.T., L.B.), by PNRR THE (Tuscany Health Ecosystem, ECS_00000017) and by a postdoctoral fellowship from the Italian Association for Cancer Research (AIRC, Projects No. 22644) awarded to L. M. The authors wish to thank Dr. Mario Chiariello (CNR, Siena, Italy) for his critical reading of the manuscript and insightful suggestions, and Dr. Jessica Costa (University of Siena, Siena, Italy) for synthesis of JC19 for the first screening. The authors are also thankful to Dr. Laura Poliseno (CNR, Pisa, Italy) for pCW-Cas9 and pLX-sgRNA plasmids, Prof. Lucia Di Marcotullio (University La Sapienza, Rome, Italy) for Glabrescione B and *Ptch1-/-* and *SuFu-/-* MEFs, Dr. Silvestro Conticello (CRL-ISPRO, Florence, Italy) for MCF10A cells, and Dr. Chiara Raggi (University of Florence, Italy) for cholangiocarcinoma cells.

Appendix A. Supporting information

Supplementary data associated with this article can be found in the online version at doi:10.1016/j.phrs.2023.106858.

References

[1] J. Jiang, Hedgehog signaling mechanism and role in cancer, Semin Cancer Biol. 85 (2022) 107–122, https://doi.org/10.1016/j.semcancer.2021.04.003.
[2] M. Varjosalo, J. Taipale, Hedgehog: functions and mechanisms, Genes Dev. 22 (2008) 2454–2472, https://doi.org/10.1101/gad.1693608.
[3] K.W. Kinzler, B. Vogelstein, The GLI gene encodes a nuclear protein which binds specific sequences in the human genome, Mol. Cell Biol. 10 (1990) 634–642, https://doi.org/10.1128/mcb.10.2.634-642.1990.
[4] N.P. Pavletich, C.O. Pabo, Crystal structure of a five-finger GLI-DNA complex: new perspectives on zinc fingers, Science 261 (1993) 1701–1707, https://doi.org/10.1126/science.8378770.
[5] D. Amakye, Z. Jagani, M. Dorsch, Unraveling the therapeutic potential of the Hedgehog pathway in cancer, Nat. Med. 19 (2013) 1410–1422, https://doi.org/10.1038/nm.3389.
[6] Y. Wang, Q. Ding, C.J. Yen, W. Xia, J.G. Izzo, J.Y. Lang, C.W. Li, J.L. Hsu, S. A. Miller, X. Wang, D.F. Lee, J.M. Hsu, L. Huo, A.M. Labaff, D. Liu, T.H. Huang, C. C. Lai, F.J. Tsai, W.C. Chang, C.H. Chen, T.T. Wu, N.S. Buttar, K.K. Wang, Y. Wu, H. Wang, J. Ajani, M.C. Hung, The crosstalk of mTOR/S6K1 and Hedgehog pathways, Cancer Cell 21 (2012) 374–387, https://doi.org/10.1016/j.ccr.2011.12.028.
[7] S.X. Atwood, M. Li, A. Lee, J.Y. Tang, A.E. Oro, GLI activation by atypical protein kinase C ι/λ regulates the growth of basal cell carcinomas, Nature 494 (2013) 484–488, https://doi.org/10.1038/nature11889.
[8] Y. Tang, S. Gholamin, S. Schubert, M.I. Willardson, A. Lee, P. Bandopadhayay, G. Bergthold, S. Masoud, B. Nguyen, N. Vue, B. Balansay, F. Yu, S. Oh, P. Woo, S. Chen, A. Ponnuswami, M. Monje, S.X. Atwood, R.J. Whitson, S. Mitra, S. H. Cheshier, J. Qi, R. Beroukhim, J.Y. Tang, R. Wechsler-Reya, A.E. Oro, B.A. Link, J.E. Bradner, Y.J. Cho, Epigenetic targeting of Hedgehog pathway transcriptional output through BET bromodomain inhibition, Nat. Med 20 (2014) 732–740, https://doi.org/10.1038/nm.3613.
[9] N.A. Riobo, G.M. Haines, C.P. Emerson Jr, Protein kinase C-delta and mitogen-activated protein/extracellular signal-regulated kinase-1 control GLI activation in hedgehog signaling, Cancer Res 66 (2006) 839–845, https://doi.org/10.1158/0008-5472.CAN-05-2539.
[10] P. Schneider, J.M. Bayo-Fina, R. Singh, P. Kumar Dhanyamraju, P. Holz, A. Baier, V. Fendrich, A. Ramaswamy, S. Baumeister, E.D. Martinez, M. Lauth, Identification of a novel actin-dependent signal transducing module allows for the targeted degradation of GLI1, Nat. Commun. 6 (2015) 8023, https://doi.org/10.1038/ncomms9023.
[11] B.K. Ehe, D.R. Lamson, M. Tarpley, R.U. Onyenwoke, L.M. Graves, K.P. Williams, Identification of a DYRK1A-mediated phosphorylation site within the nuclear localization sequence of the hedgehog transcription factor GLI1, Biochem Biophys. Res Commun. 491 (2017) 767–772, https://doi.org/10.1016/j.dib.2017.09.057.
[12] W. Gruber, M. Hutzinger, D.P. Elmer, T. Parigger, C. Sternberg, L. Cegielkowski, M. Zaja, J. Leban, S. Michel, S. Hamm, D. Vitt, F. Aberger, DYRK1B as therapeutic target in Hedgehog/GLI-dependent cancer cells with Smoothened inhibitor resistance, Oncotarget 7 (2016) 7134–7148, https://doi.org/10.18632/oncotarget.6910.
[13] Q. Shi, S. Li, S. Li, A. Jiang, Y. Chen, J. Jiang, Hedgehog-induced phosphorylation by CK1 sustains the activity of Ci/Gli activator, Proc. Natl. Acad. Sci. USA 111 (2014) E5651–E5660, https://doi.org/10.1073/pnas.1416652111.
[14] T. Purzner, J. Purzner, T. Buckstaff, G. Cozza, S. Gholamin, J.M. Rusert, T.A. Hartl, J. Sanders, N. Conley, X. Ge, M. Langan, V. Ramaswamy, L. Ellis, U. Litzenburger, S. Bolin, J. Theruvath, R. Nitta, L. Qi, X.N. Li, G. Li, M.D. Taylor, R.J. Wechsler-Reya, L.A. Pinna, Y.J. Cho, M.T. Fuller, J.E. Elias, M.P. Scott, Developmental phosphoproteomics identifies the kinase CK2 as a driver of Hedgehog signaling and a therapeutic target in medulloblastoma, Sci. Signal. 11 (2018) eaau5147, https://doi.org/10.1126/scisignal.aau5147.
[15] Z. Jagani, E.L. Mora-Blanco, C.G. Sansam, E.S. McKenna, B. Wilson, D. Chen, J. Klekota, P. Tamayo, P.T. Nguyen, M. Tolstorukov, P.J. Park, Y.J. Cho, K. Hsiao, S. Buonamici, S.L. Pomeroy, J.P. Mesirov, H. Ruffner, T. Bouwmeester, S. J. Luchansky, J. Murtie, J.F. Kelleher, M. Warmuth, W.R. Sellers, C.W. Roberts, M. Dorsch, Loss of the tumor suppressor Snf5 leads to aberrant activation of the Hedgehog-Gli pathway, Nat. Med 16 (2010) 1429–1433, https://doi.org/10.1038/nm.2251.
[16] B. Stecca, A. Ruiz i Altaba, A GLI1-p53 inhibitory loop controls neural stem cell and tumour cell numbers, EMBO J. 28 (2009) 663–676, https://doi.org/10.1038/emboj.2009.16.
[17] S. Pietrobono, S. Gagliardi, B. Stecca, Non-canonical Hedgehog Signaling Pathway in Cancer: Activation of GLI Transcription Factors Beyond Smoothened, Front Genet 10 (2019) 556, https://doi.org/10.3389/fgene.2019.00556.
[18] L. Di Marcotullio, E. Ferretti, A. Greco, E. De Smaele, A. Po, M.A. Sico, M. Alimandi, G. Giannini, M. Maroder, I. Screpanti, A. Gulino, Numb is a suppressor of Hedgehog signalling and targets Gli1 for Itch-dependent ubiquitination, Nat. Cell Biol. 8 (2006) 1415–1423, https://doi.org/10.1038/ncb1510.
[19] G. Canettieri, L. Di Marcotullio, A. Greco, S. Coni, L. Antonucci, P. Infante, L. Pietrosanti, E. De Smaele, E. Ferretti, E. Miele, M. Pelloni, G. De Simone, E. M. Pedone, P. Gallinari, A. Giorgi, C. Steinkühler, L. Vitagliano, C. Pedone, M. E. Schinin, I. Screpanti, A. Gulino, Histone deacetylase and Cullin3-REN(KCTD11) ubiquitin ligase interplay regulates Hedgehog signalling through Gli acetylation, Nat. Cell Biol. 12 (2010) 132–142, https://doi.org/10.1038/ncb2013.
[20] E. De Smaele, L. Di Marcotullio, M. Moretti, M. Pelloni, M.A. Occhione, P. Infante, D. Cucchi, A. Greco, L. Pietrosanti, J. Todorovic, S. Coni, G. Canettieri, E. Ferretti, R. Bei, M. Maroder, I. Screpanti, A. Gulino, Identification and characterization of KCASH2 and KCASH3, 2 novel Cullin3 adaptors suppressing histone deacetylase and Hedgehog activity in medulloblastoma, Neoplasia 13 (2011) 374–385, https://doi.org/10.1593/neo.101630.
[21] A.N. Mirza, M.A. Fry, N.M. Urman, S.X. Atwood, J. Roffey, G.R. Ott, B. Chen, A. Lee, A.S. Brown, S.Z. Aasi, T. Hollmig, M.A. Ator, B.D. Dorsey, B.R. Ruggeri, C. A. Zificsak, M. Sirota, J.Y. Tang, A. Butte, E. Epstein, K.Y. Sarin, A.E. Oro, Combined inhibition of atypical PKC and histone deacetylase 1 is cooperative in basal cell carcinoma treatment, JCI Insight 2 (2017), e97071, https://doi.org/10.1172/jci.insight.97071.
[22] W. Gruber, E. Peer, D.P. Elmer, C. Sternberg, S. Tesanovic, P. Del Burgo, S. Coni, G. Canettieri, D. Neureiter, R. Bartz, H. Kohlhof, D. Vitt, F. Aberger, Targeting class I histone deacetylases by the novel small molecule inhibitor 4SC-202 blocks oncogenic hedgehog-GLI signaling and overcomes smoothened inhibitor resistance, Int J. Cancer 142 (2018) 968–975, https://doi.org/10.1002/ijc.31117.
[23] N.M. Nguyen, J. Cho, Hedgehog pathway inhibitors as targeted cancer therapy and strategies to overcome drug resistance, Int J. Mol. Sci. 23 (2022) 1733, https://doi.org/10.3390/ijms23031733.
[24] S. Pietrobono, E. Gaudio, S. Gagliardi, M. Zitani, L. Carrassa, F. Migliorini, E. Petricci, F. Manetti, N. Makukhin, A.G. Bond, B.D. Paradise, A. Ciulli, M. E. Fernandez-Zapico, F. Bertoni, B. Stecca, Targeting non-canonical activation of GLI1 by the SOX2-BRD4 transcriptional complex improves the efficacy of HEDGEHOG pathway inhibition in melanoma, Oncogene 40 (2021) 3799–3814, https://doi.org/10.1038/s41388-021-01783-9.
[25] L. Vesci, F.M. Milazzo, M.A. Stasi, S. Pace, F. Manera, C. Tallarico, E. Cini, E. Petricci, F. Manetti, R. De Santis, G. Giannini, Hedgehog pathway inhibitors of the acylthiourea and acylguanidine class show antitumor activity on colon cancer in vitro and in vivo, Eur. J. Med Chem. 157 (2018) 368–379, https://doi.org/10.1016/j.ejmech.2018.07.053.
[26] S. Pietrobono, R. Santini, S. Gagliardi, F. Dapporto, D. Colecchia, M. Chiariello, C. Leone, M. Valoti, F. Manetti, E. Petricci, M. Taddei, B. Stecca, Targeted inhibition of Hedgehog-GLI signaling by novel acylguanidine derivatives inhibits melanoma cell growth by inducing replication stress and mitotic catastrophe, Cell Death Dis. 9 (2018) 142, https://doi.org/10.1038/s41419-017-0142-0.
[27] P. Infante, R. Alfonsi, B. Botta, M. Mori, L. Di Marcotullio, Targeting GLI factors to inhibit the Hedgehog pathway, Trends Pharm. Sci. 36 (2015) 547–558, https://doi.org/10.1016/j.tips.2015.05.006.
[28] J.T. Avery, R. Zhang, R.J. Boohaker, GLI1: A Therapeutic Target for Cancer, Front Oncol. 11 (2021), 673154, https://doi.org/10.3389/fonc.2021.673154.
[29] J. Kim, J.J. Lee, J. Kim, D. Gardner, P.A. Beachy, Arsenic antagonizes the Hedgehog pathway by preventing ciliary accumulation and reducing stability of

the Gli2 transcriptional effector, Proc. Natl. Acad. Sci. USA 107 (2010) 13432–13437, https://doi.org/10.1073/pnas.1006822107.
[30] E.M. Beauchamp, L. Ringer, G. Bulut, K.P. Sajwan, M.D. Hall, Y.C. Lee, D. Peaceman, M. Ozdemirli, O. Rodriguez, T.J. Macdonald, C. Albanese, J. A. Toretsky, A. Uren, Arsenic trioxide inhibits human cancer cell growth and tumor development in mice by blocking Hedgehog/GLI pathway, J. Clin. Invest 121 (2011) 148–160, https://doi.org/10.1172/JCI42874.
[31] M. Lauth, A. Bergström, T. Shimokawa, R. Toftgård, Inhibition of GLI-mediated transcription and tumor cell growth by small-molecule antagonists, Proc. Natl. Acad. Sci. USA 104 (2007) 8455–8460, https://doi.org/10.1073/pnas.0609699104.
[32] P. Infante, M. Mori, R. Alfonsi, F. Ghirga, F. Aiello, S. Toscano, C. Ingallina, M. Siler, D. Cucchi, A. Po, E. Miele, D. D'Amico, G. Canettieri, E. De Smaele, E. Ferretti, I. Screpanti, G. Uccello Barretta, M. Botta, B. Botta, A. Gulino, L. Di Marcotullio, Gli1/DNA interaction is a druggable target for Hedgehog-dependent tumors, EMBO J. 34 (2015) 200–217, https://doi.org/10.15252/embj.201489213.
[33] J. Baell, M.A. Walters, Chemistry: chemical con artists foil drug discovery, Nature 513 (2014) 481–483, https://doi.org/10.1038/513481a.
[34] S. Jasial, Y. Hu, J. Bajorath, How frequently are pan-assay interference compounds active? Large-scale analysis of screening data reveals diverse activity profiles, low global hit frequency, and many consistently inactive compounds, J. Med Chem. 60 (2017) 3879–3886, https://doi.org/10.1021/acs.jmedchem.7b00154.
[35] L. Di, E.H. Kerns, Profiling drug-like properties in discovery research, Curr. Opin. Chem. Biol. 7 (2003) 402–408, https://doi.org/10.1016/s1367-5931(03)00055-3.
[36] C.A. Lipinski, Drug-like properties and the causes of poor solubility and poor permeability, J. Pharm. Toxicol. Methods 44 (2000) 235–249, https://doi.org/10.1016/s1056-8719(00)00107-6.
[37] M. Lauth, V. Rohnalter, A. Bergström, M. Kooshesh, P. Svenningsson, R. Toftgård, Antipsychotic drugs regulate hedgehog signaling by modulation of 7-dehydrocholesterol reductase levels, Mol. Pharm. 78 (2010) 486–496, https://doi.org/10.1124/mol.110.066431.
[38] A. Agyeman, B.K. Jha, T. Mazumdar, J.A. Houghton, Mode and specificity of binding of the small molecule GANT61 to GLI determines inhibition of GLI-DNA binding, Oncotarget 5 (2014) 4492–4503, https://doi.org/10.18632/oncotarget.2046.
[39] A. Calcaterra, V. Iovine, B. Botta, D. Quaglio, I. D'Acquarica, A. Ciogli, A. Iazzetti, R. Alfonsi, L. Lospinoso Severini, P. Infante, L. Di Marcotullio, M. Mori, F. Ghirga, Chemical, computational and functional insights into the chemical stability of the Hedgehog pathway inhibitor GANT61, J. Enzym. Inhib. Med Chem. 33 (2018) 349–358, https://doi.org/10.1080/14756366.2017.1419221.
[40] P. Infante, A. Malfanti, D. Quaglio, S. Balducci, S. De Martin, F. Bufalieri, F. Mastrotto, I. Basili, M. Garofalo, L. Lospinoso Severini, M. Mori, I. Manni, M. Moretti, C. Nicoletti, G. Piaggio, P. Caliceti, B. Botta, F. Ghirga, S. Salmaso, L. Di Marcotullio, Glabrescione B delivery by self-assembling micelles efficiently inhibits tumor growth in preclinical models of Hedgehog-dependent medulloblastoma, Cancer Lett. 499 (2021) 220–231, https://doi.org/10.1016/j.canlet.2020.11.028.
[41] F. Manetti, B. Stecca, R. Santini, L. Maresca, G. Giannini, M. Taddei, E. Petricci, Pharmacophore-based virtual screening for identification of negative modulators of GLI1 as potential anticancer agents, ACS Med Chem. Lett. 11 (2020) 832–838, https://doi.org/10.1021/acsmedchemlett.9b00639.
[42] F. Manetti, L. Maresca, E. Crivaro, S. Pepe, E. Cini, S. Singh, P. Governa, S. Maramai, G. Giannini, B. Stecca, E. Petricci, Quinolines and Oxazino-quinoline Derivatives as Small Molecule GLI1 Inhibitors Identified by Virtual Screening, ACS Med Chem. Lett. 13 (2022) 1329–1336, https://doi.org/10.1021/acsmedchemlett.2c00249.
[43] R. Santini, M.C. Vinci, S. Pandolfi, J.Y. Penachioni, V. Montagnani, B. Olivito, R. Gattai, N. Pimpinelli, G. Gerlini, L. Borgognoni, B. Stecca, Hedgehog-GLI signaling drives self-renewal and tumorigenicity of human melanoma-initiating cells, Stem Cells 30 (2012) 1808–1818, https://doi.org/10.1002/stem.1160.
[44] S. Pandolfi, V. Montagnani, A. Lapucci, B. Stecca, HEDGEHOG/GLI-E2F1 axis modulates iASPP expression and function and regulates melanoma cell growth, Cell Death Differ. 22 (2015) 2006–2019, https://doi.org/10.1038/cdd.2015.56.
[45] T. Wang, J.J. Wei, D.M. Sabatini, E.S. Lander, Genetic screens in human cells using the CRISPR-Cas9 system, Science 343 (2014) 80–84, https://doi.org/10.1126/science.1246981.
[46] V. Montagnani, L. Maresca, A. Apollo, S. Pepe, R.M. Carr, M.E. Fernandez-Zapico, B. Stecca, E3 ubiquitin ligase PARK2, an inhibitor of melanoma cell growth, is repressed by the oncogenic ERK1/2-ELK1 transcriptional axis, J. Biol. Chem. 295 (2020) 16058–16071, https://doi.org/10.1074/jbc.RA120.014615.
[47] A. Brai, V. Riva, F. Saladini, C. Zamperini, C.I. Trivisani, A. Garbelli, C. Pennisi, A. Giannini, A. Boccuto, F. Bugli, M. Martini, M. Sanguinetti, M. Zazzi, E. Dreassi, M. Botta, G. Maga, DDX3X inhibitors, an effective way to overcome HIV-1 resistance targeting host proteins, Eur. J. Med Chem. 200 (2020), 112319, https://doi.org/10.1016/j.ejmech.2020.112319.
[48] C. Tintori, A. Brai, M.C. Dasso Lang, D. Deodato, A.M. Greco, B.M. Bizzarri, L. Cascone, A. Casian, C. Zamperini, E. Dreassi, E. Crespan, G. Maga, G. Vanham, E. Ceresola, F. Canducci, K.K. Ariën, M. Botta, Development and in Vitro evaluation of a microbicide gel formulation for a novel non-nucleoside reverse transcriptase inhibitor belonging to the N-Dihydroalkyloxybenzyloxopyrimidines (N-DABOs) family, J. Med Chem. 59 (2016) 2747–2759, https://doi.org/10.1021/acs.jmedchem.5b01979.
[49] M.T. Larsen, M. Kuhlmann, M.L. Hvam, K.A. Howard, Albumin-based drug delivery: harnessing nature to cure disease, Mol. Cell Ther. 4 (2016) 3, https://doi.org/10.1186/s40591-016-0048-8.
[50] C. Kilkenny, W. Browne, I.C. Cuthill, M. Emerson, D.G. Altman, NC3Rs reporting guidelines working group. animal research: reporting in vivo experiments: the ARRIVE guidelines, Br. J. Pharm. 160 (2010) 1577–1579, https://doi.org/10.1111/j.1476-5381.2010.00872.x.
[51] E. Lilley, S.C. Stanford, D.E. Kendall, S.P.H. Alexander, G. Cirino, J.R. Docherty, C. H. George, P.A. Insel, A.A. Izzo, Y. Ji, R.A. Panettieri, C.G. Sobey, B. Stefanska, G. Stephens, M. Teixeira, A. Ahluwalia, ARRIVE 2.0 and the british journal of pharmacology: updated guidance for 2020, Br. J. Pharmacol. 177 (2020) 3611–3616, https://doi.org/10.1111/bph.15178.
[52] J.K. Chen, J. Taipale, K.E. Young, T. Maiti, P.A. Beachy, Small molecule modulation of Smoothened activity, Proc. Natl. Acad. Sci. USA 99 (2002) 14071–14076, https://doi.org/10.1073/pnas.182542899.
[53] L.V. Goodrich, L. Milenković, K.M. Higgins, M.P. Scott, Altered neural cell fates and medulloblastoma in mouse patched mutants, Science 277 (1997) 1109–1113, https://doi.org/10.1126/science.277.5329.1109.
[54] J. Svärd, K. Heby-Henricson, M. Persson-Lek, B. Rozell, M. Lauth, A. Bergström, J. Ericson, R. Toftgård, S. Teglund, Genetic elimination of Suppressor of fused reveals an essential repressor function in the mammalian Hedgehog signaling pathway, Dev. Cell 10 (2006) 187–197, https://doi.org/10.1016/j.devcel.2005.12.013.
[55] L. Lospinoso Severini, D. Quaglio, I. Basili, F. Ghirga, F. Bufalieri, M. Caimano, S. Balducci, M. Moretti, I. Romeo, E. Loricchio, M. Maroder, B. Botta, M. Mori, P. Infante, L. Di Marcotullio, A Smo/Gli multitarget hedgehog pathway inhibitor impairs tumor growth, Cancers (Basel) 11 (2019) 1518, https://doi.org/10.3390/cancers11101518.
[56] V. Montagnani, B. Stecca, Role of protein kinases in hedgehog pathway control and implications for cancer therapy, Cancers (Basel) 11 (2019) 449, https://doi.org/10.3390/cancers11040449.
[57] H. Schnidar, M. Eberl, S. Klingler, D. Mangelberger, M. Kasper, C. Hauser-Kronberger, G. Regl, R. Kroismayr, R. Moriggl, M. Sibilia, F. Aberger, Epidermal growth factor receptor signaling synergizes with Hedgehog/GLI in oncogenic transformation via activation of the MEK/ERK/JUN pathway, Cancer Res 69 (2009) 1284–1292, https://doi.org/10.1158/0008-5472.CAN-08-2331.
[58] I. Galperin, L. Dempwolff, W.E. Diederich, M. Lauth, Inhibiting hedgehog: an update on pharmacological compounds and targeting strategies, J. Med Chem. 62 (2019) 8392–8411, https://doi.org/10.1021/acs.jmedchem.9b00188.
[59] R.L. Yauch, G.J. Dijkgraaf, B. Alicke, T. Januario, C.P. Ahn, T. Holcomb, K. Pujara, J. Stinson, C.A. Callahan, T. Tang, J.F. Bazan, Z. Kan, S. Seshagiri, C.L. Hann, S. E. Gould, J.A. Low, C.M. Rudin, F.J. de Sauvage, Smoothened mutation confers resistance to a Hedgehog pathway inhibitor in medulloblastoma, Science 326 (2009) 572–574, https://doi.org/10.1126/science.1179386.
[60] S. Pietrobono, B. Stecca, Targeting the oncoprotein smoothened by small molecules: focus on novel acylguanidine derivatives as potent smoothened inhibitors, Cells 7 (2018) 272, https://doi.org/10.3390/cells7120272.
[61] R.C. Dash, J. Wen, A.M. Zaino, S.R. Morel, L.Q. Chau, R.J. Wechsler-Reya, M. K. Hadden, Structure-based virtual screening identifies an 8-hydroxyquinoline as a small molecule GLI1 inhibitor, Mol. Ther. Oncolytics 20 (2021) 265–276, https://doi.org/10.1016/j.omto.2021.01.004.
[62] P. Niewiadomski, S.M. Niedziółka, Ł. Markiewicz, T. Uśpieński, B. Baran, K. Chojnowska, Gli Proteins: Regulation in Development and Cancer, Cells 8 (2019) 147, https://doi.org/10.3390/cells8020147.
[63] F. Faião-Flores, D.K. Alves-Fernandes, P.C. Pennacchi, S. Sandri, A.L. Vicente, C. Scapulatempo-Neto, V.L. Vazquez, R.M. Reis, J. Chauhan, C.R. Goding, K. S. Smalley, S.S. Maria-Engler, Targeting the hedgehog transcription factors GLI1 and GLI2 restores sensitivity to vemurafenib-resistant human melanoma cells, Oncogene 36 (2017) 1849–1861, https://doi.org/10.1038/onc.2016.348.
[64] H. Onishi, A. Fujimura, Y. Oyama, A. Yamasaki, A. Imaizumi, M. Kawamoto, M. Katano, M. Umebayashi, T. Morisaki, Hedgehog signaling regulates PDL-1 expression in cancer cells to induce anti-tumor activity by activated lymphocytes, Cell Immunol. 310 (2016) 199–204, https://doi.org/10.1016/j.cellimm.2016.08.003.
[65] J. Chakrabarti, L. Holokai, L. Syu, N.G. Steele, J. Chang, J. Wang, S. Ahmed, A. Dlugosz, Y. Zavros, Hedgehog signaling induces PD-L1 expression and tumor cell proliferation in gastric cancer, Oncotarget 9 (2018) 37439–37457, https://doi.org/10.18632/oncotarget.26473.
[66] A. Giammona, E. Crivaro, B. Stecca, Emerging roles of hedgehog signaling in cancer immunity, Int J. Mol. Sci. 24 (2023) 1321, https://doi.org/10.3390/ijms24021321.
[67] A. Otsuka, J. Dreier, P.F. Cheng, M. Nägeli, H. Lehmann, L. Felderer, I.J. Frew, S. Matsushita, M.P. Levesque, R. Dummer, Hedgehog pathway inhibitors promote adaptive immune responses in basal cell carcinoma, Clin. Cancer Res 21 (2015) 1289–1297, https://doi.org/10.1158/1078-0432.CCR-14-2110.